Intensity of Th and Pa scavenging partitioned by particle chemistry in the North Atlantic Ocean

Christopher T. Hayes[a,b,1,*], Robert F. Anderson[a,b], Martin Q. Fleisher[a], Sebastian M. Vivancos[a,b] Phoebe J. Lam[c,2], Daniel C. Ohnemus[c,3], Kuo-Fang Huang[d,4], Laura F. Robinson[c,e], Yanbin Lu[f], Hai Cheng[f,g], R. Lawrence Edwards[f], S. Bradley Moran[h]

[a]Lamont-Doherty Earth Observatory of Columbia University, Palisades, NY, USA

[b]Department of Earth & Environmental Sciences, Columbia University, New York, NY, USA

[c]Department of Marine Chemistry & Geochemistry, Woods Hole Oceanographic Institution, Woods Hole, MA, USA

[d]Department of Geology & Geophysics, Woods Hole Oceanographic Institution, Woods Hole, MA, USA

[e]School of Earth Sciences, University of Bristol, Bristol, United Kingdom

[f]Department of Earth Sciences, University of Minnesota, Minneapolis, MN, USA

[g]Institute of Global Environmental Change, Xi'an Jiaotong University, Xi'an, China

[h]Graduate School of Oceanography, University of Rhode Island, Narragansett, RI, USA

[1]Now at Department of Earth, Atmospheric and Planetary Sciences, Massachusetts Institute of Technology, Cambridge MA, USA

[2]Now at Department of Ocean Sciences, University of California, Santa Cruz, Santa Cruz, CA, USA

[3]Now at Bigelow Laboratory for Ocean Sciences, East Boothbay, ME, USA

[4]Now at Institute of Earth Sciences, Academia Sinica, Taipei, Taiwan

* corresponding author: tel: +1 (617) 324-0283, fax: +1 (617) 253-8630; Mailing address: Massachusetts Institute of Technology, Department of Earth, Atmospheric and Planetary Sciences, 45 Carleton St., E25-615,Cambridge, MA 02139, USA; Email address: cthayes@mit.edu (C. T. Hayes)

Keywords: GEOTRACES, suspended particulate matter, adsorption, radioactive tracers, trace elements

Citation: Hayes, C. T., R. F. Anderson, M. Q. Fleisher, S. M. Vivancos, P. J. Lam, D. C. Ohnemus, K.-F. Huang, L. F. Robinson, Y. Lu, H. Cheng, R. L. Edwards, S. B. Moran (2015), Intensity of Th and Pa scavenging partitioned by particle chemistry in the North Atlantic Ocean, *Marine Chemistry*, in press. doi: 10.1016/j.marchem.2015.01.006.

Abstract

The natural radionuclides ^{231}Pa and ^{230}Th are incorporated into the marine sediment record by scavenging, or adsorption to various particle types, via chemical reactions that are not fully understood. Because these isotopes have potential value in tracing several oceanographic processes, we investigate the nature of scavenging using trans-Atlantic measurements of dissolved (<0.45 μm) and particulate (0.8-51 μm) ^{231}Pa and ^{230}Th, together with major particle composition. We find widespread impact of intense scavenging by authigenic Fe/Mn (hydr)oxides, in the form of hydrothermal particles emanating from the Mid-Atlantic ridge and particles resuspended from reducing conditions near the seafloor off the coast of West Africa. Biogenic opal was not found to be a significant scavenging phase for either element in this sample set, essentially because of its low abundance and small dynamic range at the studied sites. Distribution coefficients in shallow (< 200 m) depths are anomalously low which suggests either the unexpected result of a low scavenging intensity for organic matter or that, in water masses containing abundant organic-rich particles, a greater percentage of radionuclides exist in the colloidal or complexed phase. In addition to particle concentration, the oceanic distribution of particle types likely plays a significant role in the ultimate distribution of sedimentary ^{230}Th and ^{231}Pa.

1. Introduction

The natural radionuclides ^{230}Th and ^{231}Pa are used for a variety of purposes in oceanography because of their uniform production due to U decay, their tendency to rapidly adsorb to particles (scavenging), and their sensitivity to ocean ventilation (Henderson and Anderson, 2003). Although the chemical mechanism for this scavenging is not known, radioactive disequilibria with their parent U isotopes indicate that Pa is removed by scavenging more slowly than Th (Sackett, 1960). This overall differential in scavenging intensity forms the basis of using the scavenged ^{231}Pa/^{230}Th ratio (written as Pa/Th in the text as shorthand) as a paleo-proxy, for example, of the strength of the Atlantic meridional overturning circulation (AMOC) (François, 2007; McManus et al., 2004; Yu et al., 1996).

However, it has also been shown that scavenging intensity for both elements can vary with particle type in the ocean (Anderson et al., 1983b; Chase et al., 2002; Walter et al., 1999) and in laboratory experiments (Geibert and Usbeck, 2004; Guo et al., 2002a; Lin et al., 2014; Luo and Ku, 1999). Changing proportions of particle types over geologic time may overprint other influences on the Pa/Th sediment record such as the AMOC. While previous work has demonstrated a particle composition effect on Pa/Th scavenging, there is still debate about what are the major carrier phases (Chase and Anderson, 2004; Chuang et al., 2013; Luo and Ku, 2004; Roy-Barman et al., 2009) and the importance of chemical fractionation during scavenging on basin-wide radionuclide budgets (Hayes et al., 2014; Lippold et al., 2012; Luo et al., 2010; Siddall et al., 2007). Here we present measurements of dissolved and particulate (adsorbed) ^{230}Th and ^{231}Pa from the U. S. GEOTRACES North Atlantic transect in conjunction with measurements of the mass concentration and major chemical composition of the suspended

particles. With these measurements, we calculate scavenging intensities and the degree to which Pa and Th are fractionated during scavenging in a basin-wide, analytically consistent context.

2. Approach

The chemical composition of particulate matter in the ocean has regional and depth-dependent variations. Thus, we here utilize the U. S. North Atlantic GEOTRACES Transect (Fig. 1) to observe scavenging intensities across natural variations in particle composition. Completed in two cruises, KN199-4 (GT10) and KN204-1 (GT11) are known collectively as GEOTRACES GA03. The dissolved (<0.45 μm) radionuclide (^{230}Th, ^{231}Pa) data have been described previously in a basin-wide context (Hayes et al., in press). Particulate samples were collected on Supor filters by in-situ filtration using McLane pumps (Lam et al., in press). Small particulate (0.8-51 μm) radionuclide analyses were performed by 3 inter-calibrated laboratories using methods described by Anderson et al. (2012).

In-situ pumped samples were collected with two stacked 0.8 μm Supor filters, below a 51 μm polyester screen. This protocol was designed to optimize spatial loading of particles on the filter surface, while still collecting some of the particles in the 0.45-0.8 μm size class on the bottom filter (Bishop et al., 2012). We analyzed top and bottom filters separately for a sub-set of radionuclide samples and found that radionuclides on the bottom filter were indistinguishable from "dipped" filter blanks. "Dipped" filter blanks were acid-leached filters loaded into filter holders and attached to in-situ pumps for deployment with no water pumped through them, as indicators of the in-situ pumping procedural blank. Thus, the negligible amounts of radionuclides found on the bottom filters suggests that of the small particles (0.45-51 μm), a negligible fraction of Pa or Th exist in the 0.45-0.8 μm size class. In our analyses, after initially analyzing both top

and bottom filters, subsequently only the top filter was analyzed and we consider this fraction to represent particles of size 0.8-51 µm.

The composition and mass concentration of particles collected in-situ on the cruise have also been described previously (Lam et al., in press). Briefly, separate analytical procedures were performed to measure the lithogenic material (lith), particulate organic matter (POM), calcium carbonate ($CaCO_3$), biogenic opal (opal), and authigenic $Fe(OH)_3$ and MnO_2. Lithogenic material was based on particulate Al, assuming an Al concentration in lithogenic material of 8%. POM is based on measurements of bulk, total organic carbon and does not distinguish between marine or terrestrially-derived organic carbon. Authigenic Fe and Mn phases were determined by the excess of particulate Fe and Mn over that expected from particulate Ti and assumed lithogenic Fe/Ti and Mn/Ti ratios (8.7 and 0.13, by weight respectively). Normalization to Ti, rather than Al, was used for estimating metal (hydr)oxide phases since Fe/Mn/Ti ratios were found to vary less by source region than Fe/Mn/Al ratios (Lam et al., in press; Ohnemus and Lam, in press). The chemical weight of each component was then summed to estimate the total suspended particulate matter (SPM) concentration for each filter sample (Lam et al., in press). All particle component concentrations referenced in the text are given in percent by weight.

All GEOTRACES GA03 radionuclide and particulate data are archived at the Biological and Chemical Oceanography Data Management Office (BCO-DMO, http://www.bco-dmo.org/project/2066) and the GEOTRACES International Data Assembly Center (GDAC, http://www.bodc.ac.uk/geotraces/data/). Derived scavenging parameters are tabulated in the Supplemental Material. Dissolved samples were analyzed at 16-24 depths per station and the particulate samples at 12 depths per station. If not within 10 m in the upper 1 km or within 50 m

below 1 km, we linearly interpolated the dissolved radionuclide profile onto the particulate radionuclide depths for better comparison.

The intensity parameter for scavenging is the distribution coefficient, K_d. This is defined (for Th in Eq. 1, but similarly for Pa) as the ratio of the adsorbed radionuclide (e.g., Th_{ads}^{p}) to dissolved radionuclide (Th^{d}) per unit seawater (called K), normalized by the suspended particulate matter concentration. K_d here is expressed as atoms radionuclide per gram of particulate matter over atoms radionuclide per gram of seawater (g/g). We emphasize that K_d is operationally defined in terms of its size partitioning. If the radionuclides are to any great extent adsorbed/complexed with a colloidal phase (smaller than 450 nm), the operationally defined "dissolved" concentration will be an overestimate of the truly dissolved or soluble radionuclide concentration. The apparent K_d will be biased low. Furthermore, if significant radionuclides exist in the 0.45-0.8 μm size class, our measurements of particulate radionuclides (0.8-51 μm) will underestimate the true particulate radionuclides and also contribute to a low bias in apparent K_d.

$$K_d(Th) = \frac{Th_{ads}^{p}}{Th^{d}} \times \frac{1}{SPM} = K(Th) \times \frac{1}{SPM} \qquad \left[Units: \frac{Th\ per\ g\ particles}{Th\ per\ g\ seawater}\right] \qquad \text{(Eq. 1)}$$

Adsorbed ^{230}Th ($^{230}Th_{ads}^{p}$) consists of two components (Fig. 2): the ^{230}Th that was produced by radioactive decay of dissolved ^{234}U in the water column and the ^{230}Th that was released into solution by dissolution of lithogenic minerals. Lacking evidence to the contrary, we assume that lithogenic minerals dissolve without fractionation between ^{230}Th and ^{232}Th so that the ^{230}Th/^{232}Th ratio of thorium supplied by dissolution of lithogenic minerals is equal to that of the bulk lithogenic material (4 x 10^{-6} mol/mol; Roy-Barman et al., 2009).

To calculate the adsorbed ^{230}Th, the measured particulate ^{230}Th concentration is corrected for the fraction supported by ^{234}U decay within lithogenic minerals based on measured particulate ^{232}Th (as a proxy for particulate U), and the lithogenic ^{230}Th/^{232}Th ratio (4 x 10^{-6}

mol/mol; Roy-Barman et al., 2009). Particulate ^{232}Th is used instead of ^{234}U directly, in correcting for supported ^{230}Th, because particulate U may contain an authigenic component (Anderson, 1982), which is difficult to estimate independently.

However, not all of the measured particulate ^{232}Th is bound within lithogenic material either, as some of the ^{232}Th is in the adsorbed phase (Robinson et al., 2008). In calculating the adsorbed ^{230}Th, one can take into account an adsorbed fraction of ^{232}Th, f(ads. ^{232}Th) (Eq. 2).

$$^{230}Th^{p}_{ads} = {}^{230}Th^{p}_{meas} - \left(\frac{^{230}Th}{^{232}Th}\right)_{litho} \times [1 - f(ads.\ {}^{232}Th)] \times {}^{232}Th^{p}_{meas} \qquad \text{(Eq. 2)}$$

We note here that by use of the term "adsorbed" for radionuclide concentrations, we are drawing a distinction from the particulate "excess" radionuclide, a term typically used in sedimentary geochemistry. For instance, in order to calculate the excess (or xs) particulate ^{230}Th to derive ^{230}Th-normalized sedimentary fluxes (François, 2007), one needs to correct for all of the lithogenic ^{230}Th, found either within the mineral lattice or adsorbed after originating from mineral dissolution. This procedure isolates the fraction of particulate ^{230}Th produced by uranium decay in the water column. The equation to calculate this traditional particulate excess ^{230}Th is equivalent to Eq. 2 with the adsorbed fraction of ^{232}Th set to zero. Lastly, we note that in a previous publication (Hayes et al., in press), we presented particulate ^{230}Th and ^{231}Pa data using the traditional "xs" terminology, while in fact we used Eq. 2 for the correction and these should formally be termed the adsorbed particulate concentrations. The difference between excess and adsorbed radionuclide concentrations is small (average 7% in our dataset), but nonetheless we feel refinement in the terminology is justified.

The adsorbed fraction of ^{232}Th is estimated by making an assumption that the two Th isotopes, ^{230}Th and ^{232}Th, should be subject to the same scavenging intensity, as defined by K(Th) in Eq. 1. In this way, the adsorbed component of ^{232}Th is equal to the Th distribution

coefficient multiplied by the measured dissolved ^{232}Th, which divided by the total particulate ^{232}Th, gives the adsorbed fraction of particulate ^{232}Th (Eq. 3).

$$f(ads.\,^{232}Th) = \frac{K(Th) \times {}^{232}Th^{d}}{{}^{232}Th^{p}_{meas}} = \frac{{}^{230}Th^{p}_{ads}}{{}^{230}Th^{d}} \times \frac{{}^{232}Th^{d}}{{}^{232}Th^{p}_{meas}} \quad \text{(Eq. 3)}$$

By substituting Eq. 3 into Eq. 2, the adsorbed ^{230}Th can be solved for explicitly (Eq. 4). Note that for certain applications, the dissolved ^{230}Th should also be "corrected" for a contribution from the dissolution of lithogenic material, denoted "dissolved xs" (Hayes et al., in press), but here it is appropriate to use the total dissolved ^{230}Th concentration to quantify the fraction of total particulate ^{230}Th that is adsorbed. Dissolved Th (or Pa) produced from dissolved uranium decay or by mineral dissolution will equally participate in scavenging reactions; that is, we assume that all adsorbed Th (and Pa) participates in reversible adsorption exchange reactions with the dissolved phase (Bacon and Anderson, 1982), and thus is relevant to the evaluation of scavenging intensity (K_d). By contrast, we assume that "detrital" or lattice-bound ^{230}Th and ^{231}Pa, the fraction of each isotope produced by radioactive decay of U bound within the structure of lithogenic minerals, does not participate in exchange reactions with the dissolved nuclides.

$${}^{230}Th^{p}_{ads} = \frac{{}^{230}Th^{p}_{meas} - \left(\frac{{}^{230}Th}{{}^{232}Th}\right)_{litho} \times {}^{232}Th^{p}_{meas}}{1 - \left(\frac{{}^{230}Th}{{}^{232}Th}\right)_{litho} \times \frac{{}^{232}Th^{d}}{{}^{230}Th^{d}}} \quad \text{(Eq. 4)}$$

To calculate the adsorbed ^{231}Pa, we use a lithogenic ^{231}Pa/^{232}Th ratio of 8.8 x 10^{-8} mol/mol (Taylor and McLennan, 1995), and the adsorbed fraction of ^{232}Th (Eq. 5). The fractions of particulate ^{230}Th and ^{231}Pa supported by uranium decay bound within lithogenic material ranged from 0-60% depending on water depth (adsorbed ^{230}Th and ^{231}Pa concentrations generally increase with water depth) and lithogenic content (see Fig. S1). The fraction of particulate ^{232}Th in the adsorbed phase was 30-40% in most cases, consistent with previous estimates (Robinson et al. 2008).

$$^{231}Pa^{p}_{ads} = {}^{231}Pa^{p}_{meas} - \left(\frac{^{231}Pa}{^{232}Th}\right)_{litho} \times [1 - f(ads.\ {}^{232}Th)] \times {}^{232}Th^{p}_{meas} \quad \text{(Eq. 5)}$$

In order to statistically interpret the variations in K_d values with respect to particle composition, we consider each measured K_d a linear sum of contributions from each major particle phase (lith, $CaCO_3$, opal, POM, $Fe(OH)_3$, MnO_2) (cf.Li (2005)). Each contribution is the product of the K_d for a pure end-member phase (unknown), weighted by its fraction of the total mass of a particle sample (Eq. 6).

$$K_d = f(lith) * K_d^{lith} + f(CaCO_3) * K_d^{CaCO_3} + f(opal) * K_d^{opal} + f(POM) * K_d^{POM}$$
$$+ f(Fe(OH)_3) * K_d^{Fe(OH)_3} + f(MnO_2) * K_d^{MnO_2} \quad \text{(Eq. 6)}$$

This is done for each particle sample (e.g., sample 1, 2, 3, etc. in Eq. 7) and the pure end-member K_d's can be solved for using a non-negative least-squares regression (since a negative K_d is not physically meaningful). We estimate uncertainty in the derived end-member K_d values using the range of values obtained in regressing jackknifed resampling of the data, i.e., iteratively excluding each sample from the data pool.

$$\begin{bmatrix} K_d^1 \\ K_d^2 \\ K_d^3 \\ \dots \end{bmatrix} = \begin{bmatrix} f(lith)^1\ f(CaCO_3)^1\ f(opal)^1\ f(POM)^1\ f(Fe(OH)_3)^1\ f(MnO_2)^1 \\ f(lith)^2\ f(CaCO_3)^2\ f(opal)^2\ f(POM)^2\ f(Fe(OH)_3)^2\ f(MnO_2)^2 \\ f(lith)^3\ f(CaCO_3)^3\ f(opal)^3\ f(POM)^3\ f(Fe(OH)_3)^3\ f(MnO_2)^3 \\ \dots \end{bmatrix} \times \begin{bmatrix} K_d^{lith} \\ K_d^{CaCO_3} \\ K_d^{opal} \\ K_d^{POM} \\ K_d^{Fe(OH)_3} \\ K_d^{MnO_2} \end{bmatrix}$$

(Eq. 7)

Finally, we estimate the degree to which Th and Pa are fractionated during scavenging using the fractionation factor, F(Th/Pa) (Anderson et al., 1983b), which is the intensity of Th scavenging relative to that of Pa (Eq. 8) or ratio of the corresponding K_d's. Note that in calculating F(Th/Pa) from the definition of K_d given in equation 1, the SPM term will cancel.

Thus the fractionation factor is nominally independent of particle concentration and only a function of particle composition. F(Th/Pa) may, however, be subject to a bias related to size-partitioning if Th and Pa exist in a colloidal phase at differing proportions.

$$F\left(\frac{Th}{Pa}\right) = \frac{K_d(Th)}{K_d(Pa)} = \frac{Th_{ads}^{p}}{Th^{d}} \div \frac{Pa_{ads}^{p}}{Pa^{d}} \qquad \text{(Eq. 8)}$$

3. Results

3.1 Distribution coefficient estimates

The estimates of K_d(Th) and K_d(Pa) across the North Atlantic transect (Fig. 3A, 3B) have logarithmic changes of a similar spatial structure for both elements. The lowest K_d's are found in the upper 400 m. The highest K_d's are found near bottom at the mid-Atlantic ridge (GT11-16) and off the Mauritanian margin (GT10-09). In several instances, such as the Mediterranean Outflow around 1 km depth at GT10-01, or near bottom between Woods Hole, MA and Bermuda (GT11-01→GT11-10, also known as Line W), an inverse relationship can be observed between SPM (Fig. 3C) and K_d. This relationship has been termed the "particle concentration effect" (Honeyman et al., 1988; Moran and Buesseler, 1993) and is interpreted to reflect a greater proportion of colloidal radionuclides, thus producing lower apparent K_d's, in high SPM waters. While particle concentration effect can explain a large part of the observed K_d variability, the particle chemistry at the aforementioned extremes in K_d values signal how both particle concentration and composition determine Th and Pa scavenging.

In Figure 4 we put the K_d observations into the context of the major particle components. These data are sorted by increasing K_d(Th) (Fig. 4A), showing the percent-weight composition of the major particle components (Fig. 4B) and the SPM for each sample (Fig. 4C). With a few exceptions, the particle samples are primarily mixtures of lithogenic material, $CaCO_3$, and POM. Opal was consistently a relatively minor component (0-17%). Generally, increasing K_d values

are associated with increasing lithogenic content, decreasing POM content, and decreasing SPM (Figs. 4C, S2, S3).

The highest K_d values (~10^8 g/g for Th and 10^7 g/g for Pa, Fig. 3) can be immediately associated with unique particle chemistry (Fig. 4, sample numbers 207-211 in Fig. 4). At GT11-16, also known as the TAG hydrothermal site, a hydrothermal plume was observed at ~3.3 km depth and the particulate material in and surrounding it were 8-52% authigenic Fe hydroxide (but interestingly no Mn oxide enrichment was observed there). At station GT10-09 near Mauritania, two near-bottom samples were taken within a layer of resuspended sediments containing ~2% each of $Fe(OH)_3$ and MnO_2 (samples 198, 204 in Fig. 4). Metal (hydr)oxide enrichments clearly enhance the scavenging of both Th and Pa.

Another interesting anomaly in this dataset comes from the bottom several samples along Line W, where relatively particle-laden nepheloid layers (SPM = 100-1200 µg/kg) were observed, largely of lithogenic composition (within sample numbers 145-175 in Fig. 4). Despite SPM values orders of magnitude above the oceanic background (5-10 µg/kg), the measured K_d values for Th and Pa were still in the typical range of observed deep water values (Figs. 3, 4).

3.2 Particle concentration effect

Plotting the measured K_d values against SPM from GA03 (Fig. 5), one can observe the trends predicted by a simple particle concentration effect. In log-log space, K_d values decrease with increasing SPM. The "anomalies" to the linear trends in Fig. 5 are closely related to unique particle chemistry. Many of the particle samples falling below the apparent trends are characterized by >60% organic matter. Samples falling above the trends are characterized by significant (>1%) weight percent of authigenic Fe and Mn (hydr)oxides (from stations GT11-16 and GT10-09), or the benthic samples from Line W which are largely composed of resuspended

lithogenic material but with total SPM concentrations orders of magnitude higher than the rest of the transect.

After excluding these three compositional groups (>60% POM, authigenic Fe/Mn present, and lithogenic nepheloid layers), the linear trends are Log K_d(Th) [g/g] = 7.78 – 0.66 * Log SPM [µg/kg] (R^2 = 0.53, $p < 0.001$) and Log K_d(Pa) = 6.63 – 0.66 * Log SPM [µg/kg] (R^2 = 0.39, $p < 0.001$). The regression for Th is remarkably similar to previous compilations of K_d(Th) measurements (Henderson et al., 1999; Honeyman et al., 1988), taken from oceanic to coastal settings, implying that the particle concentration effect may be a universal factor in Th scavenging. The particle concentration effect has been shown to affect the size-partitioning of many trace metals, such as Al, Pb, Hg, and Fe (Moran and Moore, 1989; Moran et al., 1996) and to our knowledge this is the first study documenting the particle concentration effect in-situ for Pa.

Recent experimental work (Chuang et al., 2013; Lin et al., 2014) determined K_d(Th) values generally consistent with the trend in Fig. 5. These studies had experimental conditions with much higher SPM concentrations (10-50 mg/kg) than those reported here from GA03. For the case of Pa, however, the K_d(Pa) values determined by Lin et al. (2014) and Chuang et al. (2013) are 1 to 2 orders of magnitude higher than predicted by the particle concentration trend found here (Fig. 5) for reasons we cannot fully explain. Recreating in the laboratory the oceanic conditions for trace metal scavenging is certainly challenging, and the observational approach from GEOTRACES is also limited to some extent by operational size-class definitions. The logarithmic range of experimentally determined Th- and Pa- K_d values, nonetheless, is similar to the range from our North Atlantic survey (Fig. 5), which in both the observational and experimental approaches can be largely attributed to particle chemistry. Phase-specific

scavenging intensities in some cases override the apparently global particle concentration effect. We make a first attempt at attribution to specific phases using the described statistical analysis (Sec. 4.1).

3.3 Fractionation factor F(Th/Pa) estimates

The fact that the relative changes in K_d(Th) and K_d(Pa) values track each other quite closely (Fig 2, Fig. 4A) is representative of a relatively uniform fractionation factor across the transect (10-20, mean ~15). There is nonetheless a significant trend of the fractionation factor with depth (Fig. 6A). The highest F(Th/Pa) values are found shallower than 1 km depth, particularly for the more interior sites. The upper water column (< 1 km), however, also has the greatest variability and analytical uncertainty (20-30%) in fractionation factor. The analytical uncertainty is large in part because error propagation in calculating F(Th/Pa) results in the compounding of analytical error from 6 separate analyses (Eqs. 4, 8). The largest contributor to the error (in shallow waters especially) is from the particulate ^{231}Pa analysis for which the sample size in some cases approaches our limit of detection as defined by 3 standard deviations of ^{231}Pa in "dipped" Supor filter blanks (0.30 µBq ^{231}Pa, n = 23 across the three participating labs).

Below 1 km depth, the fractionation factor generally decreases with depth for nearly all stations (Fig. 6A) as has been observed in the equatorial and south Atlantic (Moran et al., 2002). The lowest F(Th/Pa) values obtained are 6-7 in the Fe and Mn (hydr)oxide enrichment at the bottom of the Mauritanian margin station, GT10-09. That the fractionation factor generally decreases with depth is a reflection of the character of the scavenging particles having an increasing affinity to scavenge Pa relative to Th. Although throughout the whole water column Th is clearly preferentially scavenged over Pa by a factor of more than 7 at these sites, the

preferential scavenging of Th over Pa is reduced with depth. Either the deep particles have a smaller affinity to scavenge Th or a greater affinity to scavenge Pa, the latter appearing more consistent with the K_d data (Fig. 3). Additionally, some (but not all) of the variation in F(Th/Pa) seems to coincide with the spatial variation in the particulate opal/$CaCO_3$ ratio (Fig. 6B), a ratio which has been found to be a significant determinant for the particulate Pa/Th ratio (cf. Fig. 6C) of sediment trap material (Chase et al., 2002). Again here we defer to the described statistical regression of K_d values (Sec. 4.1) in order to more precisely define the role of particle composition in fractionation.

We put the fractionation factor observations into a wider Atlantic context with previously published results in Figure 7. Plotting all the water column observations as a function of latitude, one can see that throughout the (sub)tropical Atlantic (40°N-40°S) the fractionation factor is nearly always above 5. The results from the equatorial and subtropical South Atlantic (Moran et al., 2002; Scholten et al., 2008) have a range in F(Th/Pa) which is consistent with that observed in the North Atlantic transect. It appears that only at high northern latitudes, such as the Labrador Sea (Moran et al., 2002), and south of 50°S (Walter et al., 1997), does F(Th/Pa) become lower than 5. Lower fractionation factors at high latitudes have been attributed to increased contents of biogenic opal, given its special affinity to scavenge Pa (Moran et al., 2002; Walter et al., 1999) presumably because diatoms are more prevalent in nutrient-rich, (sub)polar waters.

If the lower F(Th/Pa) values at high latitudes are assumed to result from increased K_d(Pa), one can infer a longer water column residence time for Pa throughout the (sub)tropical Atlantic (because it is removed less intensely there). This is significant for its paleo-proxy applications in that mid- and low-latitude Pa would be more sensitive than high-latitude Pa to redistribution by circulation, either by advection or eddy diffusion. However, decreased values of

F(Th/Pa) at high latitude could also result from lower K_d(Th) values (with no change in K_d(Pa)), as some studies have determined the K_d(Th) for opal is particularly low (Chase et al., 2002; Siddall et al., 2005). This caveat highlights the value of analyzing SPM in addition to dissolved and particulate radionuclides to be able to consider the geographic variation in K_d(Th) and K_d(Pa) separately. This presentation of the fractionation data (Fig. 7) may also be somewhat misleading since the plotted sites are largely from the interior ocean. If more sites were included from high productivity upwelling sites near the coast or along the equator where diatoms are more prevalent, lower fractionation factors may be observed at low latitudes as well.

4. Discussion

4.1 End-member distribution coefficient regressions

The results of the non-negative least squares regression between the measured K_d's for Th and Pa and the particle component concentrations are listed in Table 1. A general caveat in interpreting the results of this regression is that the variability in the observed K_d's is assumed to be a function of particle composition. We have seen already that particle concentration, and potentially particle size, appear to influence K_d to some extent independently of particle composition. Nonetheless, this regression provides a first step in attributing scavenging intensity to specific particle phases insofar as these data allow. For visual inspection of the correlations, the K_d and particle composition data are cross-plotted for Th (Fig. S2) and Pa (Fig. S3). Significant end-member K_d values could not be derived for opal for either Th or Pa. This may be due in part to the fact that opal concentrations were generally low and had a small dynamic range in this study.

Derived end-member K_d's for lithogenics, $CaCO_3$, POM, MnO_2 and $Fe(OH)_3$ span 4 orders of magnitude (Table 1). The derived end-member fractionation factors, calculated as the

ratio of end-member K_d(Th) to end-member K_d(Pa), ranges from 5 to 33. Strong fractionation, associated with the adsorption of Th relative to Pa, for lithogenics and $CaCO_3$ is consistent with previous work (Chase et al., 2002; Geibert and Usbeck, 2004). F(Th/Pa) equal to 33 ± 15 for $CaCO_3$ makes it likely that this phase contributes to the highest F(Th/Pa) values of 20-30, observed in the upper 1000 m (Fig. 6) of the North Atlantic.

The K_d values for Fe and Mn (hydr)oxides (10^8-10^9 g/g for Th, 10^7-10^8 g/g for Pa) are orders of magnitude above those for lithogenics and $CaCO_3$ (~10^7 g/g for Th, ~10^6 g/g for Pa), confirming the clear enhanced scavenging intensity in section view (Fig. 3). The MnO_2 K_d values reported here are much larger than what has been determined experimentally (Geibert and Usbeck, 2004; Guo et al., 2002a), but are consistent with measured K_d values from the Panama Basin where there are enrichments of MnO_2 in the surface sediments (1-2% MnO_2), similar to that observed at station GT10-09 near Mauritania (Anderson et al., 1983a). Additionally, Roy-Barman et al. (2009) estimated an even higher K_d(Th) for MnO_2 of 60-110 x 10^8 g/g based on sediment traps from the Mediterranean Sea.

These observations suggest that authigenic MnO_2 formed naturally may be more reactive toward adsorption than as a pure phase. In oceanic settings, MnO_2 primarily occurs as microbially-mediated coatings (Cowen and Bruland, 1985), providing much higher reactive surface area than afforded by pure phases. This finding has implications for the biogeochemical modeling of trace metals in that the end-member K_d values derived in this paper are not truly representative of pure phases (e.g., MnO_2), but they are the correct end-member values to use practically since they incorporate the influence of physical form (surface coatings) as well as chemical affinity of marine particles.

The enhanced intensity of scavenging by $Fe(OH)_3$ is not surprising given the known influence of intensified scavenging by hydrothermal plume particles (German et al., 1991). What is surprising is that the fractionation factors estimated for MnO_2 (6 ± 3) and $Fe(OH)_3$ (11 ± 6) (Table 1) imply a strong preference for scavenging Th over Pa. Previous work, on the other hand, has concluded that these phases do not fractionate the two elements during scavenging, with F(Th/Pa) = 1 (Anderson et al., 1983b). Experimental studies have also found F(Th/Pa) close to 1 for manganese oxides, but for iron hydroxides F(Th/Pa) was determined as 4-5 (Geibert and Usbeck, 2004; Guo et al., 2002a). De-convolving the observed distribution coefficients using particle composition in terms of reactive surface area rather than weight percentage may help explain these discrepancies. The measurement of reactive surface area of undisturbed oceanic particles, however, presents a great analytical challenge, and it may be that oceanic K_d and F(Th/Pa) values will always be influenced by operational definitions.

Opal concentrations in the particle samples studied were small (generally below 10%, Fig. 4B) and the dynamic range in opal concentration was also small, less than 10. Therefore this dataset does not allow for a direct test of the hypothesis that sedimentary Pa/Th ratios in the North Atlantic can be overprinted by large variations in opal scavenging (Keigwin and Boyle, 2008). We can conclude, however, that opal was not a major scavenging phase of Th or Pa along this North Atlantic transect since no statistically significant end-member K_d could be derived for opal.

There is a possibility that our sampling suffers from a seasonal bias. In the Sargasso Sea diatoms are generally only a very small proportion of the phytoplankton community, but their greatest abundances occur during winter/spring blooms (Nelson and Brzezinski, 1997). The upwelling that leads to diatom blooms off the coast of Mauritania also occurs seasonally,

typically in June-July (Santos et al., 2005). Our sampling took place in late fall (Oct-Dec), missing the productive season for diatoms in both the east and west. We would expect the variation in particle composition associated with diatom blooms to occur mostly in the upper water column (< 1000 m), however, since deep sediment traps (3200 m) from the Ocean Flux Program site (near station GT11-10) have recorded nearly constant opal composition (~15 ± 3% opal) for more than 10 years (Conte et al., 2001).

While we conclude that opal is not a major carrier phase of Pa in the North Atlantic, our data are largely consistent with the log-log correlation between the opal/$CaCO_3$ ratio and particulate Pa/Th ratio found by Chase et al. (2002) (Figs. 6B, 6C, 8). The North Atlantic Transect points fall only on the low side of the opal/$CaCO_3$-Pa/Th ratio correlation. In fact, very few of the particulate Pa/Th ratio observations from this study fall above the activity ratio initially produced by U decay (0.093) (Figs. 6C, 8). Furthermore, the good agreement between the results of this study and the global compilation suggests that a cause for the low particulate Pa/Th ratios is the low opal/$CaCO_3$ ratios of North Atlantic particles (Honjo et al., 2008). This explanation, however, may only hold for the subtropical North Atlantic in which most of our observations are made. In the subtropics, picoplankton and $CaCO_3$-producing coccolithophorids are favored in primary production over microplankton such as opal-producing diatoms. Further work in the subarctic and equatorial Atlantic may lend support to the hypothesis that large-scale regimes exist with distinct Pa/Th fractionation coinciding with biogeographic provinces (Hayes et al., 2014; Longhurst, 2006).

POM concentrations appeared to generally have an inverse relationship with K_d(Th) and K_d(Pa) (Figs. 4, S2, S3). This finding is at odds with experimental and observational work that suggests very high sorption affinities, relative to inorganic substrates, for Th and Pa of organic

macromolecules such as polysaccharides containing extracellular polymeric substances (EPS) (e.g., (Guo et al., 2002b; Quigley et al., 2002; Roberts et al., 2009; Santschi et al., 2006)). Of course, in this bulk phase analysis, we cannot detect the influence of any minor organic phases that may not correlate with bulk POM. In the next section (4.2) we explore the possibility that the finding of low K_d values for Th and Pa may actually be an artifact related to increased proportions of colloidal Th and Pa associated with high POM surface waters.

As a way of attributing the importance of particle types to scavenging, we calculate the contribution of each individual particle phase to the total observed scavenging intensity (K_d) (end-member K_d for phase x, multiplied by the concentration of phase x in the particle sample, divided by the total predicted K_d for the particle sample). In this presentation of the data (Fig. 9), the major carrier phases (largest contributions to the total K_d) of both Th (Fig. 9A) and Pa (Fig. 9B) in the North Atlantic are lithogenic material and $CaCO_3$, with POM rivaling the contribution made by $CaCO_3$ for Pa. Interestingly, the K_d(Pa) for MnO_2 is so high (2.1×10^8 g/g) that even at the low MnO_2 concentrations of the typical particles (0.1-0.3%), we estimate that this phase is contributing ~15% of overall Pa scavenging (Fig. 9B). Finally, $Fe(OH)_3$ is clearly the dominant scavenging phase for both elements in the hydrothermal plume samples (Fig. 9, sample nos. >206).

The results presented in Table 1 and Figure 9 help bring closure to the debate about the major carrying phases of Th and Pa (Chase and Anderson, 2004; Chase et al., 2002; Luo and Ku, 1999; Luo and Ku, 2004; Roy-Barman et al., 2005; Roy-Barman et al., 2009). Lithogenic material and $CaCO_3$ both bind Th and Pa with a higher intensity than POM, but all three intensities are still within the same order of magnitude (Table 1). The majority of Pa and Th scavenging can be attributed to lithogenic and $CaCO_3$ (Fig. 9B, 9C); however, all phases, with

the exception of opal, contribute significantly to scavenging, depending on the location, as proposed by Li (2005). Fe and Mn (hydr)oxides bind Th and Pa with intensity 1-3 orders of magnitude higher than the other major components (Table 1). The low abundance of these phases (generally < 1%) results in a modest contribution to total Th and Pa scavenging (Fig. 9), excepting locations of redox chemistry such as hydrothermal plume or reducing surface sediments.

The significant contribution of Fe/Mn (hydr)oxides to total scavenging has important implications for the paleo-proxy application of sedimentary Pa and Th distributions. Given the ubiquity of metal (hydr)oxide enrichment in deep-sea surface sediments, scavenging reactions at or below the water-sediment interface could overprint any chemical signature acquired in the water column. We find an analogy here with another scavenged-type paleo-proxy metal, neodymium, whose isotopic composition is used to trace water mass provenance. The Nd isotope signature of fossil planktic foraminifera have been interpreted to reflect bottom water Nd, as opposed to Nd acquired in the upper water column, due to the predominance of scavenged Nd in the Fe-Mn oxide coatings of the shells (Roberts et al., 2010).

4.2 The colloid conspiracy

In the vein of Turekian's "great particle conspiracy" (1977) in which sorption/scavenging processes were revealed to play a dominant role in the cycling of trace metals in the ocean, in this section we discuss the possibility that colloidal organic matter plays a dominant role in scavenging Th and Pa in shallow waters. While we have no measurements on colloidal organic matter, the largest POM content is found in the upper 200 m (POM = 60-80% of the total particle mass), coincident with the lowest measured K_d values as well as relatively high SPM content

(10-20 µg/kg) (Figs. 3, 4). On this basis, we raise the possibility that increased colloidal Th and Pa are found in high POM surface ocean environments.

An increasing proportion of colloidal radionuclides at high SPM (and POM) contents has already been implicated by the fact that measured K_d values for the high POM samples (>60%) are even lower than expected from the global particle concentration effect (Fig. 5). Low apparent K_d values could also be the result of low molecular weight dissolved organic molecules with high complexation capacities which essentially stabilize Th (or Pa) in solution (Barbeau et al., 2001). This would be consistent with the finding of elevated Th complexation capacity confined to the upper 200-300 m of the ocean (Hirose et al., 2011; Hirose and Tanoue, 1994; Hirose and Tanoue, 1998) and is difficult to distinguish from the colloidal hypothesis with the available data.

Our finding that K_d values for resuspended sediments fall far above the particle concentration effect line (Fig. 5) also supports the hypothesis that surface-ocean-derived organic phases (dissolved or colloidal) influence the scavenging behavior of Th and Pa. The western boundary nepheloid layers we sampled were found in oxidizing conditions and most likely lacked freshly produced colloidal/dissolved organic complexing agents, which may explain the absence of the particle concentration effect. Similarly, our K_d results for resuspended sediments are much higher than K_d's from laboratory experiments run at comparable SPM concentrations (Fig. 5). There are many factors possibly responsible for this discrepancy such as differing particle composition, differing particle size spectra, or ageing of particles between scavenging observations in natural versus artificial settings. When dealing with potentially unique combinations of particle sizes and composition, such as near the seafloor, in-situ observation most likely provides the most accurate approach to investigate scavenging intensity and provides

the appropriate quantitative values of scavenging parameters to be coded into global ocean models of Th and Pa biogeochemistry.

Low shallow water K_d values could be due to a truly lower K_d end-member value associated with organic matter, the colloidal effect described above, or some combination of the two. If one assumes the low shallow water K_d's are artifacts entirely related to colloids, and that the more uniform K_d values in mid- to deep water (1-3 km depth) are unaffected by colloids, then one can estimate the fraction of "dissolved" radionuclide that would have to be found in the colloidal/complexed phase, f(colloid), by mass balance. Essentially, f(colloid) is proportional to the relative deviation of the measured K_d (Eq. 9). Assuming a "colloid-free" K_d(Th) = 1.5 x 10^7 g/g, the dissolved phase of ^{230}Th as measured is implied to be, at a maximum, 80-90% colloidal/complexed. Most shallow samples are estimated between 30-60% colloidal/complexed. A similar result, f(colloid) = 20-90%, is obtained for ^{231}Pa (assuming a "colloid-free" K_d(Pa) = 2 x 10^6 g/g). Of course, these are maximum estimates and if organic matter truly has a lower K_d than other particle types (Table 1), then the cited colloidal fractions will be overestimates. The assumption that deep water radionuclides are "colloid-free" may also be incorrect. If the deep sea dissolved Th or Pa did contain a substantial colloidal fraction, then the theoretical "colloid-free" K_d would be even larger, and the f(colloid) estimates would be larger than estimated above.

$$f(colloid) = 1 - \frac{measured\ K_d}{colloid-free\ K_d} \qquad \text{Eq. 9}$$

Very little work on colloidal ^{230}Th (or ^{231}Pa) has been done, but colloidal ^{234}Th (reviewed by Guo and Santschi (2007)) has received attention for its application in quantifying organic matter export. The colloidal fraction of dissolved ^{234}Th has been estimated to occur over a large range (0-78%), but generally, f(colloid) values for ^{234}Th greater than 50% have been found only in near-shore waters with SPM concentrations on the order of 100 mg/kg. Thus the estimated 80-

90% colloidal fractions of ^{230}Th (^{231}Pa) reported here for oceanic waters may be surprising results, although, as stated above, these could be overestimates if POM truly has a lower K_d than the other major particle types. Future work to determine the size partitioning of ^{230}Th would be helpful in understanding the scavenging removal of Th in shallow waters, which is of particular relevance for the use of dissolved ^{232}Th fluxes based on ^{230}Th scavenging removal as a tracer of lithogenic inputs (Deng et al., 2014; Hayes et al., 2013; Hsieh et al., 2011).

The statistical approach employed here to attribute scavenging to particle types would be improved with information on the sub-micron size-partitioning of the radionuclides and/or major components. Additionally, rather than simply using the quantity of POM, characterizing the types (quality) of POM, which may differ in their scavenging tendencies (poly acid saccharides, proteins, lipids, etc.), may reveal more information about the locations of the most intense scavenging by organic matter.

5. Conclusions

In this study, lithogenic material and $CaCO_3$ are major carrier phases of scavenged Th and Pa in the North Atlantic Ocean. Mn and Fe (hydr)oxide phases have scavenging intensities orders of magnitude larger than the other major particle components for both Th and Pa, and metal (hydr)oxides can be major scavenging phases at certain sites. These include hydrothermal vents and near-shore environments where sediments undergo redox cycling due to high rates of organic matter respiration, creating Fe and/or Mn (hydr)oxide coatings on other particulate phases. Even at very low MnO_2 concentrations (such as the oxide coatings of clay), this phase contributes significantly to Pa scavenging (~15%), perhaps in part due to the high surface activity of this phase in the ocean.

In our sampling, opal was not a major phase of the particle samples (< 15%) and could not be correlated with an increase in Pa scavenging intensity. In the modern subtropical Atlantic, sedimentary Pa/Th ratios are most likely not heavily influenced by opal scavenging, with the caveat that the impact of seasonal opal production could not be assessed in this synoptic case.

Anomalously low K_d values in shallow water (< 200 m) with the highest POM content intimate the possibility that organic colloids or dissolved organic complexing agents play a significant role in scavenging/complexing both radionuclides. Scavenging at greater depths is attributed largely to inorganic phases. Future work should pursue the seasonal variability of particle composition and scavenging intensities (as determined by in-situ pumps), size-fractionation of dissolved ^{230}Th and ^{231}Pa to determine the role of colloids, and further characterization of POM (and possibly colloidal OM) to determine which organic compounds are associated with the highest scavenging intensities, as well as their spatial extent.

Acknowledgements

Cruise management for GA03 was funded by the U. S. National Science Foundation to W. Jenkins (OCE-0926423), E. Boyle (OCE-0926204), and G. Cutter (OCE-0926092). Radionuclide studies were supported by NSF (OCE-0927064 to LDEO, OCE-0926860 to WHOI, OCE-0927757 to URI, and OCE-0927754 to UMN). Additional support came from the European Research Council (278705) to LFR and the Ford Foundation Predoctoral Fellowship to SMV. Particle studies were supported by NSF OCE-0963026 to PJL. The crew of the R/V *Knorr*, the Ocean Data Facility team (Mary Johnson, Rob Palomares, Susan Becker, and Courtney Schatzman), and the science team samplers for Niskin bottles and in-situ pumps (Katharina Pahnke, Brett Longworth, Paul Morris, Kuanbo Zhou, Sylvain Rigaud and Stephanie Owens) are all acknowledged for their critical roles in the success of these cruises. Figures 1, 3, 6 and S1 were created using Ocean Data View (Schlitzer, 2014). Maureen Auro and Joanne Goudreau are thanked for sample preparation efforts. We thank three anonymous reviewers for critical and constructive reviews. This is LDEO contribution 7867.

Figure Captions

Figure 1. Map of the sites from the US GEOTRACES North Atlantic cruises (red diamonds) reported on in this study. GT11-01→GT11-10 represents seven closely packed stations, GT11-01, GT11-02, GT11-03, GT11-04, GT11-06, GT11-08, and GT11-10, between Woods Hole, MA and Bermuda. Data from other sites referred to in the text were reported by Moran et al. (2002)

(black squares), Walter et al. (1997) (green triangles), Scholten et al. (2008) (purple x's) and Chase et al (2002) (blue dots).

Figure 2. Components of measured ^{230}Th in marine particulate material ($^{230}Th^{p}_{meas}$). The majority of particulate ^{230}Th is adsorbed on to particle surfaces having originated from the decay of uranium dissolved in seawater. This component is typically considered particulate excess ($^{230}Th^{p}_{xs}$) and is represented above as the solid blue bar coating the marine particle. Two smaller fractions of particulate ^{230}Th originate from the decay of uranium within the lattices of lithogenic minerals. The sum of these two fractions, represented by the blue dots within the marine particle plus the red-hashed blue bar coating the particle, is typically considered the "supported" fraction in sediment geochemistry. When lithogenic minerals enter the ocean, they partially dissolve. Dissolution of minerals therefore releases some of this "supported" ^{230}Th into solution which subsequently leads to some adsorbed ^{230}Th originating from mineral dissolution (red-hashed blue bar). The motivation for these distinctions is that in considering adsorption-desorption reactions between seawater and marine particles, it is the total adsorbed component (blue bar plus red-hashed blue bar, or $^{230}Th^{p}_{ads}$) which is relevant. In contrast, for deriving rates with respect to seawater uranium decay, such as sedimentary fluxes, one should use the particulate excess component. While illustrated above for ^{230}Th, equivalent components exist for particulate ^{231}Pa. See section 2 for equations detailing these parameters.

Figure 3. Vertical sections of the distribution coefficient (K_d) for (A) ^{230}Th and (B) ^{231}Pa and (C) suspended (0.8-51 µm) particulate matter (SPM) concentration from GA03, the U.S. GEOTRACES North Atlantic Transect (inset map).

Figure 4. (A) K_d results for all samples analyzed in this study sorted by increasing K_d(Th) (red diamonds). Note the corresponding K_d(Pa) values (blue triangles) (A) are on their own, offset scale on the right. (B) Corresponding particle compositions (% weights of lithogenic material, $CaCO_3$, biogenic opal, particulate organic matter, MnO_2 and $Fe(OH)_3$) (Lam et al., in press) and (C) suspended particulate matter concentrations of the particle samples (Lam et al., in press) ordered in the same way as (A).

Figure 5. Log-log scatter plots of (A) K_d(Th) and (B) K_d(Pa) versus suspended particulate matter (SPM) concentration from our study sites. While there is a general trend for decreasing K_d values at higher SPM, samples with >60% POM, samples for which metal (hydr)oxide scavenging is significant (GT11-16 and GT10-09), and samples from benthic nepheloid layers of resuspended, mostly lithogenic, sediment do not fall on the least-squares fit trend of the rest of the samples (solid line). The particle concentration effect curves determined from previous compilations by Honeyman et al. (1988) and Henderson et al. (1999) are shown for Th. Also shown are data from recent experimental determination of K_d using tracer additions in laboratory-prepared suspensions (Chuang et al., 2013; Lin et al., 2014).

Figure 6. Vertical sections along GA03, the U. S. GEOTRACES North Atlantic transect (as in Fig. 3) of (A) the fractionation factor, F(Th/Pa), (B) the opal to calcium carbonate ratio of suspended particulate matter, (C) the adsorbed particulate ^{231}Pa/^{230}Th ratio, and (D) the dissolved ^{231}Pa/^{230}Th ratio. The ^{231}Pa/^{230}Th ratio produced initially by U decay in seawater is 0.093. Note in (B), for data marked with a white circle (GT10-3, -5, -7, and 4 deepest samples of GT10-1), direct $CaCO_3$ measurements were suspect. $CaCO_3$ for these samples was instead estimated from

measurements of total particulate carbon and a fixed particulate inorganic carbon to total particulate carbon ratio (Lam et al., in press). These estimated $CaCO_3$ values were not used in statistical interpretation of the composition data (i.e., Figs. 4B, 8, 9, S2, S3 or Table 1).

Figure 7. Fractionation factors, F(Th/Pa), calculated between seawater and suspended particles in the water column, determined from the U.S. GEOTRACES North Atlantic transect (red diamonds) compared with published estimates reported by Moran et al. (2002), Walter et al. (1997), and Scholten et al. (2008) as a function of latitude in the Atlantic. See Figure 1 for station locations.

Figure 8. The ratio of adsorbed $^{231}Pa/^{230}Th$ versus the particulate opal to $CaCO_3$ ratio on suspended particles from GA03, the U.S. GEOTRACES North Atlantic Transect, in red diamonds compared with particulate xs $^{231}Pa/^{230}Th$ and opal/$CaCO_3$ of global sediment trap material (Chase et al. 2002) in blue dots. See Fig. 1 for station locations. Note that both axes are log-scale and that the data from Chase et al. are calculated using traditional excess radionuclide concentrations rather than formally adsorbed (see Sec. 2), but this difference is very small (on the order of 1% in our dataset) since both numerator and denominator are corrected in the same way. The horizontal dotted line represents the $^{231}Pa/^{230}Th$ activity ratio produced initially by U decay in seawater (0.093).

Figure 9. The fractional contribution of the major particle components to the total scavenging of (A) Th and (B) Pa in comparison to (C) particle composition in weight percent (Lam et al., in press) (sample number ordered by increasing K_d(Th)). White bars in (B) represent samples for which K_d(Th) data exist but K_d(Pa) data do not because particulate ^{231}Pa was below detection. Opal does not have a significant contribution in any of the samples in (A) or (B) since a statistically-significant end-member K_d could not be derived in the non-negative least squares regression (Sec. 4).

Figure captions for Supplemental Material

Figure S1. Vertical sections along GA03, the U.S. GEOTRACES North Atlantic transect (as in Figs. 2, 5) of (A) adsorbed particulate ^{230}Th, (B) adsorbed particulate ^{231}Pa and the percentage composition of total particulate (C) ^{230}Th and (D) ^{231}Pa which is "detrital", or found within mineral lattices (as opposed to scavenged from seawater). Several points are labelled where values exceed the color bar ranges.

Figure S2. Cross-plots of K_d(Th) versus the particulate matter content of (A) lithogenic material, (B) opal, (C) $CaCO_3$, (D) particulate organic matter, (E) manganese oxides, and (F) iron hydroxides (F). Plot insets denote the Pearson linear correlation coefficient (r) and two-tailed p-value (statistical significance is usually attributed when p is less than 0.05). Note, however, that negative correlation coefficients are not physically meaningful as this would imply a negative K_d for pure phases. These apparent negative relationships must arise from the mixing of phases with different scavenging affinities. We therefore refer the reader to the non-negative, multiple least squares regression presented in the main text with regard to attributing scavenging intensity to specific phases.

Figure S3. Cross-plots of K_d(Pa) versus the particulate matter content of (A) lithogenic material, (B) opal, (C) $CaCO_3$, (D) particulate organic matter, (E) manganese oxides, and (F) iron hydroxides. Plot insets denote the Pearson linear correlation coefficient (r) and two-tailed p-value (statistical significance is usually attributed when p is less than 0.05). Note, however, that negative correlation coefficients are not physically meaningful as this would imply a negative K_d for pure phases. These apparent negative relationships must arise from the mixing of phases with different scavenging affinities. We therefore refer the reader to the non-negative, multiple least squares regression presented in the main text with regard to attributing scavenging intensity to specific phases.

References

Anderson, R.F., 1982. Concentration, vertical flux, and remineralization of particulate uranium in seawater. Geochim. Cosmochim. Acta, 46(7): 1293-1299.

Anderson, R.F., Bacon, M.P. and Brewer, P.G., 1983a. Removal of ^{230}Th and ^{231}Pa at ocean margins. Earth Planet. Sci. Lett., 66: 73-90.

Anderson, R.F., Bacon, M.P. and Brewer, P.G., 1983b. Removal of ^{230}Th and ^{231}Pa from the open ocean. Earth Planet. Sci. Lett., 62(1): 7-23.

Anderson, R.F. et al., 2012. GEOTRACES intercalibration of ^{230}Th, ^{232}Th, ^{231}Pa, and prospects for ^{10}Be. Limnol. Oceanogr. Methods, 10: 179-213.

Bacon, M.P. and Anderson, R.F., 1982. Distribution of thorium isotopes between dissolved and particulate forms in the deep sea. J. Geophys. Res., 87(C3): 2045-2056.

Barbeau, K., Kujawinski, E.B. and Moffett, J.W., 2001. Remineralization and recycling of iron, thorium and organic carbon by heterotrophic marine protists in culture. Aquat. Microb. Ecol., 24(1): 69-81.

Bishop, J.K., Lam, P.J. and Wood, T.J., 2012. Getting good particles: Accurate sampling of particles by large volume in-situ filtration. Limnol. Oceanogr. Methods, 10: 681-710.

Chase, Z. and Anderson, R.F., 2004. Comment on "On the importance of opal, carbonate, and lithogenic clays in scavenging and fractionating ^{230}Th, ^{231}Pa and ^{10}Be in the ocean" by S. Luo and T.-L. Ku. Earth Planet. Sci. Lett., 220(1-2): 213-222.

Chase, Z., Anderson, R.F., Fleisher, M.Q. and Kubik, P.W., 2002. The influence of particle composition and particle flux on scavenging of Th, Pa and Be in the ocean. Earth Planet. Sci. Lett., 204(1-2): 215-229.

Chuang, C.-Y. et al., 2013. Role of biopolymers as major carrier phases of Th, Pa, Pb, Po, and Be radionuclides in settling particles from the Atlantic Ocean. Mar. Chem., 157(0): 131-143.

Conte, M.H., Ralph, N. and Ross, E.H., 2001. Seasonal and interannual variability in deep ocean particle fluxes at the Oceanic Flux Program (OFP)/Bermuda Atlantic Time Series (BATS) site in the western Sargasso Sea near Bermuda. Deep-Sea Res. II, 48(8–9): 1471-1505.

Cowen, J.P. and Bruland, K.W., 1985. Metal deposits associated with bacteria: implications for Fe and Mn marine biogeochemistry. Deep-Sea Res. A, 32(3): 253-272.

Deng, F., Thomas, A.L., Rijkenberg, M.J.A. and Henderson, G.M., 2014. Controls on seawater ^{231}Pa, ^{230}Th and ^{232}Th concentrations along the flow paths of deep waters in the Southwest Atlantic. Earth Planet. Sci. Lett., 390(0): 93-102.

François, R., 2007. Paleoflux and Paleocirculation from Sediment ^{230}Th and ^{231}Pa/^{230}Th. In: C. Hillaire-Marcel and A. de Vernal (Editors), Developments in Marine Geology. Elsevier, pp. 681-716.

Geibert, W. and Usbeck, R., 2004. Adsorption of thorium and protactinium onto different particle types: experimental findings. Geochim. Cosmochim. Acta, 68(7): 1489-1501.

German, C.R., Fleer, A.P., Bacon, M.P. and Edmond, J.M., 1991. Hydrothermal scavenging at the Mid-Atlantic Ridge: radionuclide distributions. Earth Planet. Sci. Lett., 105(1–3): 170-181.

Guo, L., Chen, M. and Gueguen, C., 2002a. Control of Pa/Th ratio by particulate chemical composition in the ocean. Geophys. Res. Lett., 29(20): 1961.

Guo, L., Hung, C.-C., Santschi, P.H. and Walsh, I.D., 2002b. ^{234}Th scavenging and its relationship to acid polysaccharide abundance in the Gulf of Mexico. Mar. Chem., 78(2–3): 103-119.

Guo, L. and Santschi, P.H., 2007. Ultrafiltration and its applications to sampling and characterisation of aquatic colloids. IUPAC Series on Analytical and Physical Chemistry of Environmental Systems, 10: 159.

Hayes, C.T. et al., in press. ^{230}Th and ^{231}Pa on GEOTRACES GA03, the U.S. GEOTRACES North Atlantic transect, and implications for modern and paleoceanographic chemical fluxes. Deep-Sea Res. II, Available online: http://www.sciencedirect.com/science/article/pii/S0967064514001799.

Hayes, C.T. et al., 2013. Quantifying lithogenic inputs to the North Pacific Ocean using the long-lived thorium isotopes. Earth Planet. Sci. Lett., 383: 16-25.

Hayes, C.T. et al., 2014. Biogeography in ^{231}Pa/^{230}Th ratios and a balanced ^{231}Pa budget for the Pacific Ocean. Earth Planet. Sci. Lett., 391: 307-318.

Henderson, G.M. and Anderson, R.F., 2003. The U-series Toolbox for Paleoceanography. Rev. Mineral. Geochem., 52(1): 493-531.

Henderson, G.M., Heinze, C., Anderson, R.F. and Winguth, A.M.E., 1999. Global distribution of the ^{230}Th flux to ocean sediments constrained by GCM modelling. Deep-Sea Res. I, 46(11): 1861-1893.

Hirose, K., Saito, T., Lee, S.H. and Gastaud, J., 2011. Vertical distributions of the strong organic ligand in the twilight zone of Southern Hemisphere Ocean particulate matter. Prog. Oceanogr., 89(1–4): 108-119.

Hirose, K. and Tanoue, E., 1994. Thorium-particulate matter interaction. Thorium complexing capacity of oceanic particulate matter: Theory. Geochim. Cosmochim. Acta, 58(1): 1-7.

Hirose, K. and Tanoue, E., 1998. The vertical distribution of the strong ligand in particulate organic matter in the North Pacific. Mar. Chem., 59(3–4): 235-252.

Honeyman, B.D., Balistrieri, L.S. and Murray, J.W., 1988. Oceanic trace metal scavenging: the importance of particle concentration. Deep-Sea Res. A, 35(2): 227-246.

Honjo, S., Manganini, S.J., Krishfield, R.A. and Francois, R., 2008. Particulate organic carbon fluxes to the ocean interior and factors controlling the biological pump: A synthesis of global sediment trap programs since 1983. Prog. Oceanogr., 76(3): 217-285.

Hsieh, Y.-T., Henderson, G.M. and Thomas, A.L., 2011. Combining seawater ^{232}Th and ^{230}Th concentrations to determine dust fluxes to the surface ocean. Earth Planet. Sci. Lett., 312(3–4): 280-290.

Keigwin, L.D. and Boyle, E.A., 2008. Did North Atlantic overturning halt 17,000 years ago? Paleoceanography, 23(1): PA1101.

Lam, P.J., Ohnemus, D.C. and Auro, M.E., in press. Size fractionated major particle composition and concentration from the US GEOTRACES North Atlantic Zonal Transect. Deep-Sea Res. II, Available Online: http://dx.doi.org/10.1016/j.dsr2.2014.11.020.

Li, Y.-H., 2005. Controversy over the relationship between major components of sediment-trap materials and the bulk distribution coefficients of ^{230}Th, ^{231}Pa, and ^{10}Be. Earth Planet. Sci. Lett., 233(1-2): 1-7.

Lin, P., Guo, L. and Chen, M., 2014. Adsorption and fractionation of thorium and protactinium on nanoparticles in seawater. Mar. Chem., 162(0): 50-59.

Lippold, J. et al., 2012. Strength and geometry of the glacial Atlantic Meridional Overturning Circulation. Nat. Geosci., 5(11): 813-816.

Longhurst, A., 2006. Ecological Geography of the Sea. Academic Press, San Diego, 560 pp.

Luo, S. and Ku, T.-L., 1999. Oceanic ^{231}Pa/^{230}Th ratio influenced by particle composition and remineralization. Earth Planet. Sci. Lett., 167(3-4): 183-195.

Luo, S. and Ku, T.-L., 2004. On the importance of opal, carbonate, and lithogenic clays in scavenging and fractionating ^{230}Th, ^{231}Pa and ^{10}Be in the ocean. Earth Planet. Sci. Lett., 220(1-2): 201-211.

Luo, Y., Francois, R. and Allen, S.E., 2010. Sediment ^{231}Pa/^{230}Th as a recorder of the rate of the Atlantic meridional overturning circulation: insights from a 2-D model. Ocean Sci., 6(1): 381-400.

McManus, J.F., Francois, R., Gherardi, J.M., Keigwin, L.D. and Brown-Leger, S., 2004. Collapse and rapid resumption of Atlantic meridional circulation linked to deglacial climate changes. Nature, 428(6985): 834-837.

Moran, S.B. and Buesseler, K.O., 1993. Size-fractionated ^{234}Th in continental shelf waters off New England: Implications for the role of colloids in oceanic trace metal scavenging. J. Mar. Res., 51(4): 893-922.

Moran, S.B. and Moore, R.M., 1989. The distribution of colloidal aluminum and organic carbon in coastal and open ocean waters off Nova Scotia. Geochim. Cosmochim. Acta, 53(10): 2519-2527.

Moran, S.B. et al., 2002. Dissolved and particulate ^{231}Pa and ^{230}Th in the Atlantic Ocean: constraints on intermediate/deep water age, boundary scavenging, and ^{231}Pa/^{230}Th fractionation. Earth Planet. Sci. Lett., 203(3-4): 999-1014.

Moran, S.B., Yeats, P.A. and Balls, P.W., 1996. On the role of colloids in trace metal solid-solution partitioning in continental shelf waters: a comparison of model results and field data. Cont. Shelf Res., 16(3): 397-408.

Nelson, D.M. and Brzezinski, M.A., 1997. Diatom growth and productivity in an oligotrophic midocean gyre: A 3-yr record from the Sargasso Sea near Bermuda. Limnol. Oceanogr., 42(3): 473-486.

Ohnemus, D.C. and Lam, P.J., in press. Cycling of lithogenic marine particulates in the US GEOTRACES North Atlantic Zonal Transect. Deep-Sea Res. II, Available Online: http://dx.doi.org/10.1016/j.dsr2.2014.11.019.

Quigley, M.S., Santschi, P.H., Hung, C.-C., Guo, L. and Honeyman, B.D., 2002. Importance of acid polysaccharides for ^{234}Th complexation to marine organic matter. Limnol. Oceanogr., 47(2): 367-377.

Roberts, K.A., Xu, C., Hung, C.-C., Conte, M.H. and Santschi, P.H., 2009. Scavenging and fractionation of thorium vs. protactinium in the ocean, as determined from particle-water partitioning experiments with sediment trap material from the Gulf of Mexico and Sargasso Sea. Earth Planet. Sci. Lett., 286(1-2): 131-138.

Roberts, N.L., Piotrowski, A.M., McManus, J.F. and Keigwin, L.D., 2010. Synchronous Deglacial Overturning and Water Mass Source Changes. Science, 327(5961): 75-78.

Robinson, L.F., Noble, T.L. and McManus, J.F., 2008. Measurement of adsorbed and total ^{232}Th/^{230}Th ratios from marine sediments. Chem. Geol., 252(3-4): 169-179.

Roy-Barman, M. et al., 2005. The influence of particle composition on thorium scavenging in the NE Atlantic ocean (POMME experiment). Earth Planet. Sci. Lett., 240(3–4): 681-693.

Roy-Barman, M. et al., 2009. The influence of particle composition on thorium scavenging in the Mediterranean Sea. Earth Planet. Sci. Lett., 286(3–4): 526-534.

Sackett, W.M., 1960. Protactinium-231 content of ocean water and sediments. Science, 132: 1761-1762.

Santos, A.M.P., Kazmin, A.S. and Peliz, Á., 2005. Decadal changes in the Canary upwelling system as revealed by satellite observations: Their impact on productivity. J. Mar. Res., 63(2): 359-379.

Santschi, P.H. et al., 2006. Thorium speciation in seawater. Mar. Chem., 100(3–4): 250-268.

Schlitzer, R., 2014. http://odv.awi.de.

Scholten, J.C. et al., 2008. Advection and scavenging: Effects on ^{230}Th and ^{231}Pa distribution off Southwest Africa. Earth Planet. Sci. Lett., 271(1-4): 159-169.

Siddall, M. et al., 2005. $^{231}Pa/^{230}Th$ fractionation by ocean transport, biogenic particle flux and particle type. Earth Planet. Sci. Lett., 237(1-2): 135-155.

Siddall, M. et al., 2007. Modeling the relationship between $^{231}Pa/^{230}Th$ distribution in North Atlantic sediment and Atlantic meridional overturning circulation. Paleoceanography, 22(2): PA2214.

Taylor, S.R. and McLennan, S.M., 1995. The geochemical evolution of the continental crust. Rev. Geophys., 33(2): 241-265.

Turekian, K.K., 1977. The fate of metals in the oceans. Geochim. Cosmochim. Acta, 41(8): 1139-1144.

Walter, H.-J., Rutgers v. d. Loeff, M.M. and Francois, R., 1999. Reliability of the $^{231}Pa/^{230}Th$ Activity Ratio as a Tracer for Bioproductivity of the Ocean. In: W. Fischer and G. Wefer (Editors), Use of Proxies in Paleoceanography: Examples for the South Atlantic. Springer-Verlag, Berlin, pp. 393-408.

Walter, H.J., Rutgers van der Loeff, M.M. and Hoeltzen, H., 1997. Enhanced scavenging of ^{231}Pa relative to ^{230}Th in the South Atlantic south of the Polar Front: Implications for the use of the $^{231}Pa/^{230}Th$ ratio as a paleoproductivity proxy. Earth Planet. Sci. Lett., 149(1-4): 85-100.

Yu, E.-F., Francois, R. and Bacon, M.P., 1996. Similar rates of modern and last-glacial ocean thermohaline circulation inferred from radiochemical data. Nature, 379(6567): 689-694.

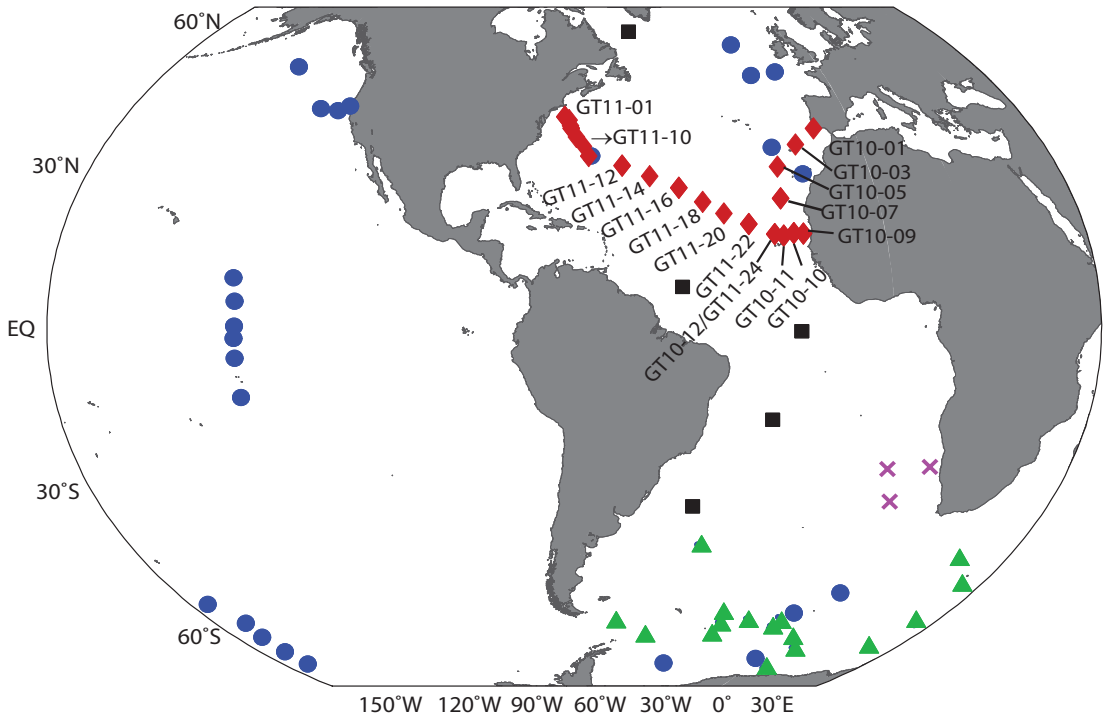
60°N
30°N
EQ
30°S
60°S
150°W
120°W
90°W
60°W
30°W
0°
30°E
GT11-01
→GT11-10
GT11-12
GT11-14
GT11-16
GT11-18
GT11-20
GT11-22
GT11-24/GT10-12
GT10-11
GT10-10
GT10-01
GT10-03
GT10-05
GT10-07
GT10-09

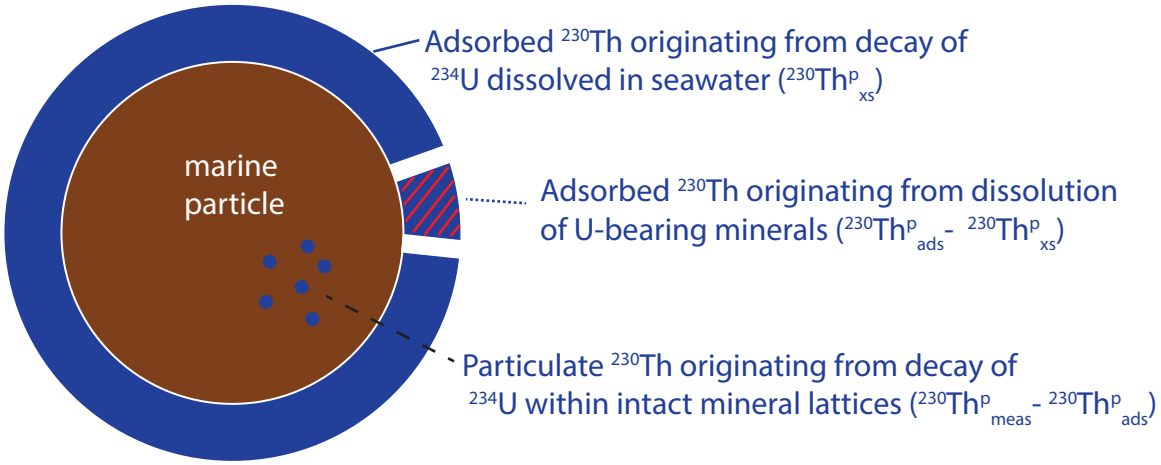
marine
particle
Adsorbed ^{230}Th originating from decay of ^{234}U dissolved in seawater ($^{230}Th^{p}_{xs}$)
Adsorbed ^{230}Th originating from dissolution of U-bearing minerals ($^{230}Th^{p}_{ads}$ - $^{230}Th^{p}_{xs}$)
Particulate ^{230}Th originating from decay of ^{234}U within intact mineral lattices ($^{230}Th^{p}_{meas}$ - $^{230}Th^{p}_{ads}$)

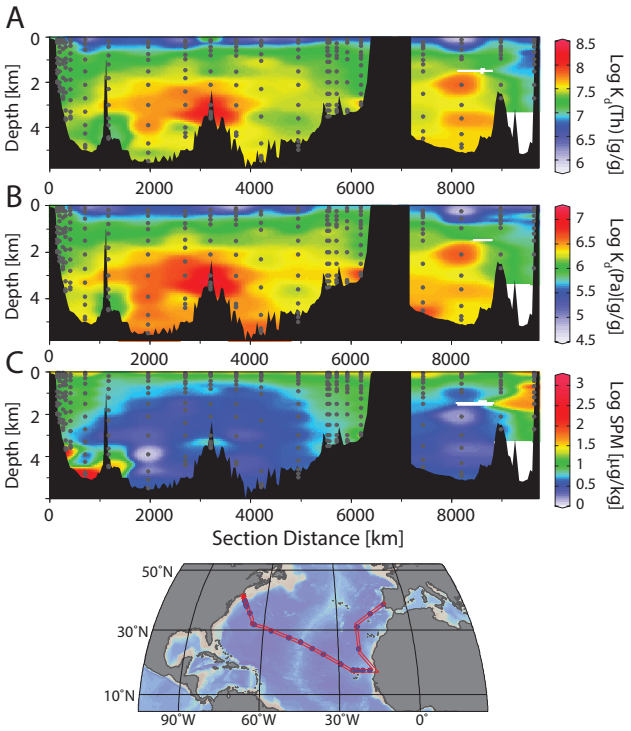
A
B
C
Depth [km]
0
2
4
0
2000
4000
6000
8000
Section Distance [km]
Log K_d(Th) [g/g]
8.5
8
7.5
7
6.5
6
Log K_d(Pa)[g/g]
7
6.5
6
5.5
5
4.5
Log SPM [µg/kg]
3
2.5
2
1.5
1
0.5
0
50°N
30°N
10°N
90°W
60°W
30°W
0°

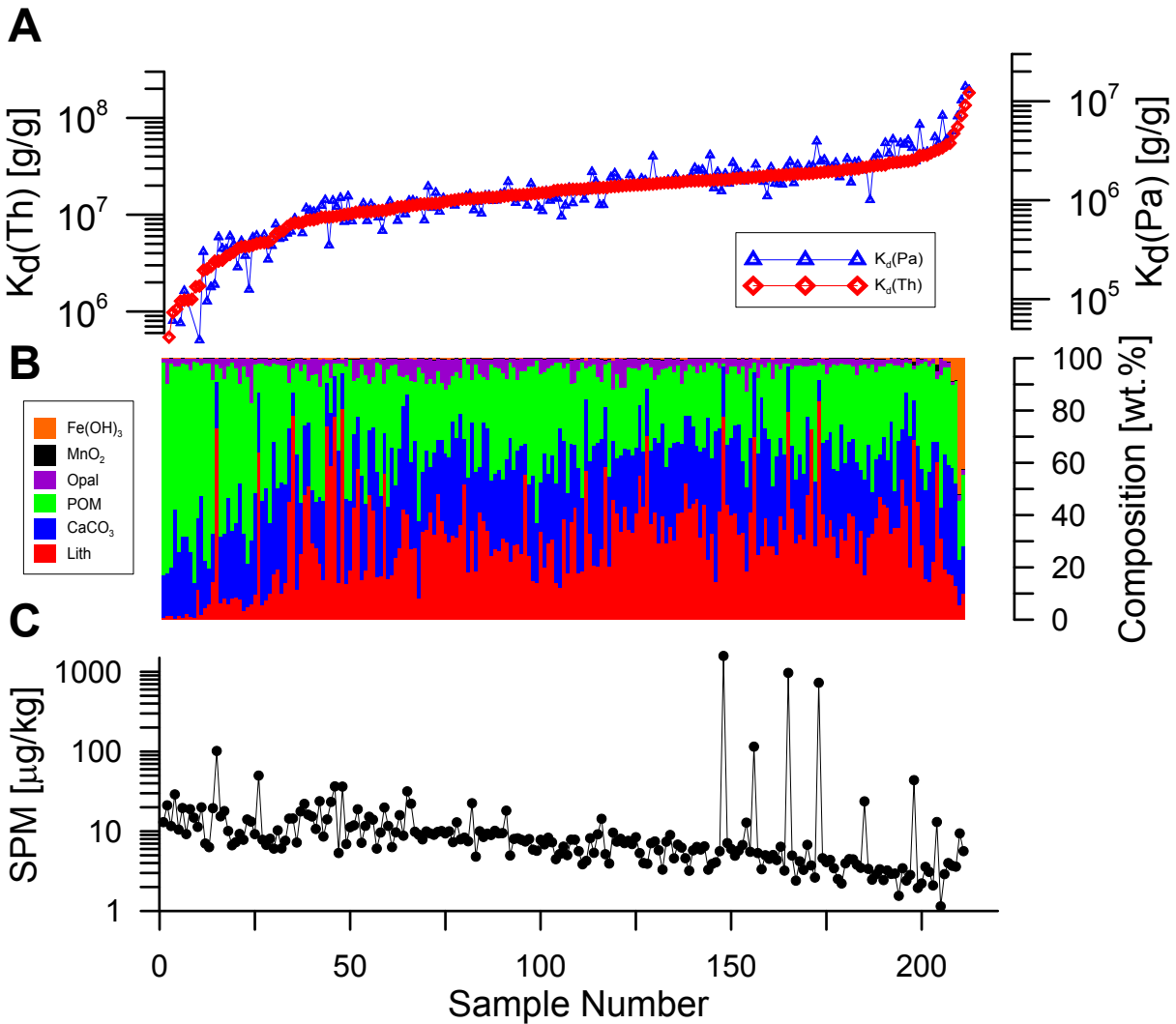
A
B
C
K_d(Th) [g/g]
K_d(Pa) [g/g]
K_d(Pa)
K_d(Th)
Fe(OH)$_3$
MnO$_2$
Opal
POM
CaCO$_3$
Lith
Composition [wt.%]
SPM [µg/kg]
Sample Number

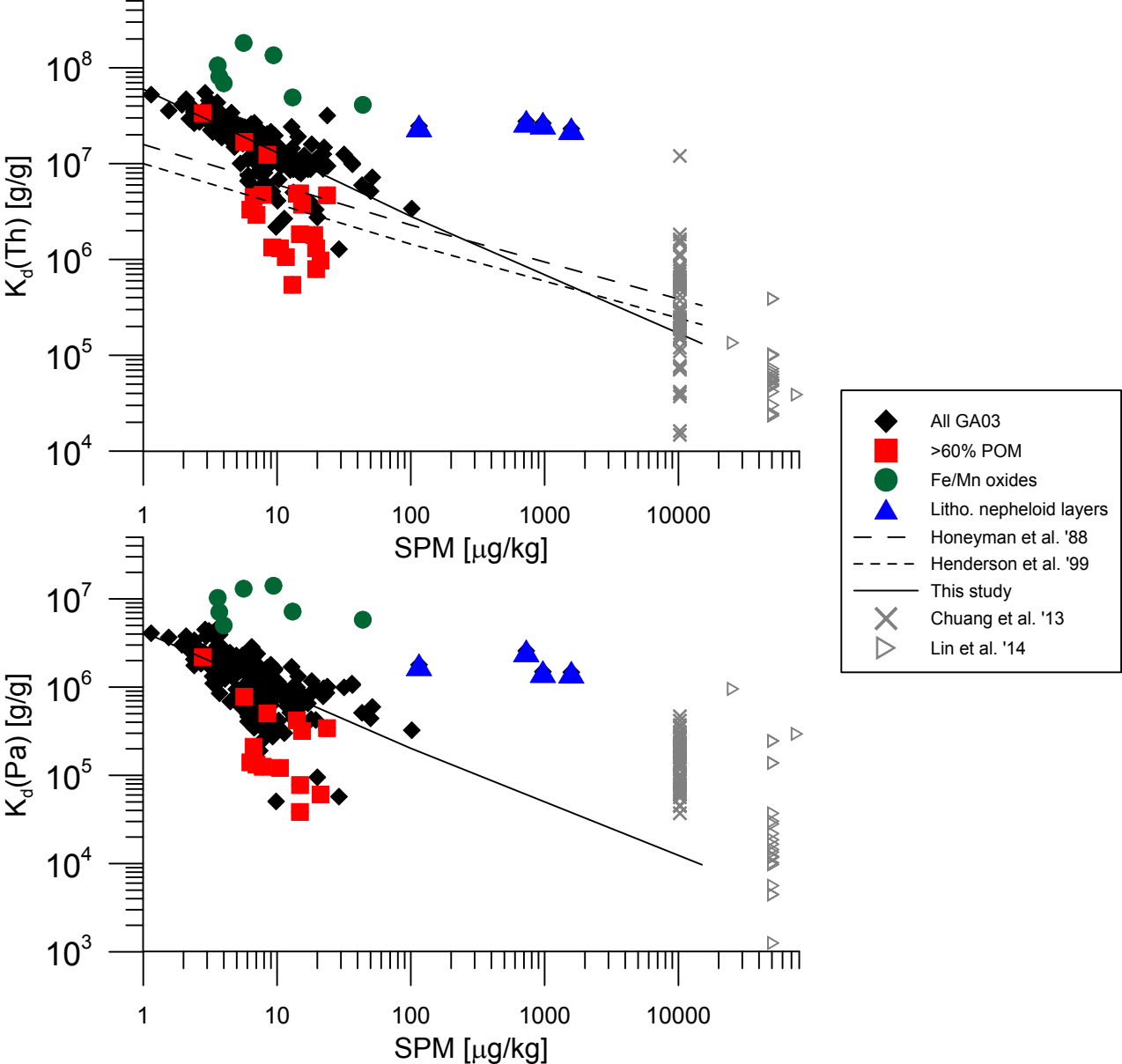
K_d(Th) [g/g]
10^8
10^7
10^6
10^5
10^4
1
10
100
1000
10000
SPM [μg/kg]
K_d(Pa) [g/g]
10^7
10^6
10^5
10^4
10^3
1
10
100
1000
10000
SPM [μg/kg]
All GA03
>60% POM
Fe/Mn oxides
Litho. nepheloid layers
Honeyman et al. '88
Henderson et al. '99
This study
Chuang et al. '13
Lin et al. '14

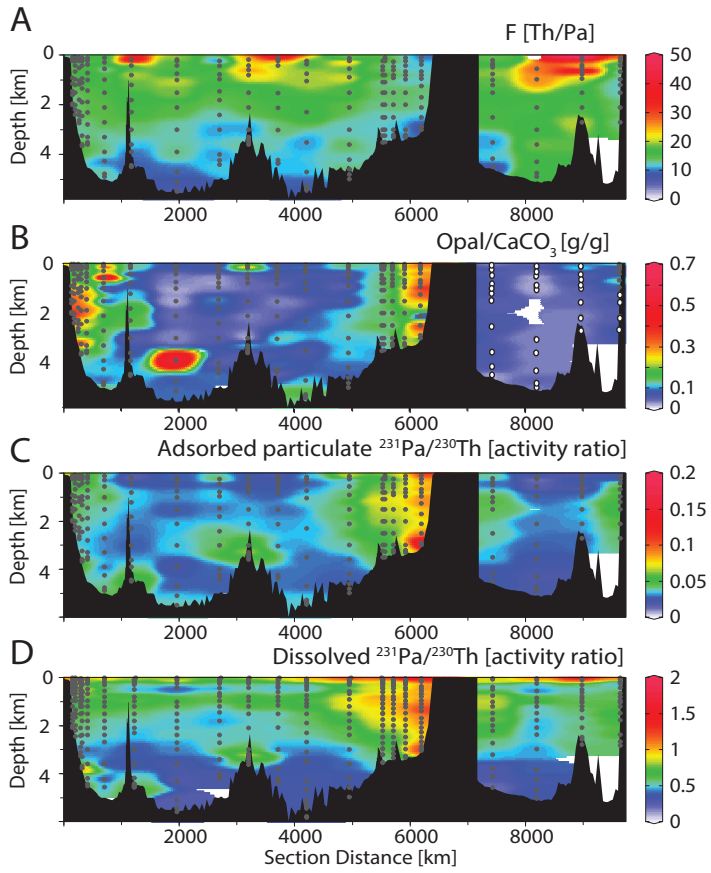
A
F [Th/Pa]
Depth [km]
0
2
4
2000
4000
6000
8000
50
40
30
20
10
0
B
Opal/CaCO3 [g/g]
0.7
0.5
0.3
0.1
0
C
Adsorbed particulate 231Pa/230Th [activity ratio]
0.2
0.15
0.1
0.05
0
D
Dissolved 231Pa/230Th [activity ratio]
2
1.5
1
0.5
0
Section Distance [km]

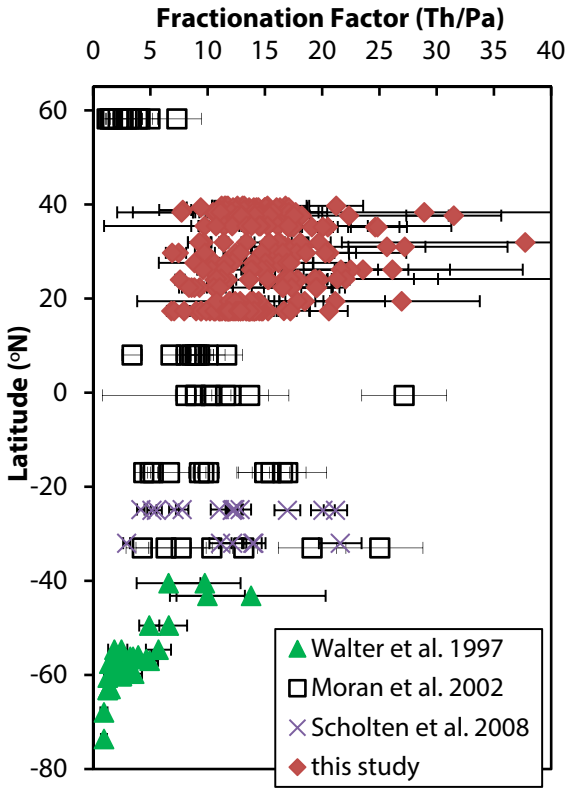
Fractionation Factor (Th/Pa)
0
5
10
15
20
25
30
35
40
60
40
20
0
-20
-40
-60
-80
Latitude (°N)
Walter et al. 1997
Moran et al. 2002
Scholten et al. 2008
this study

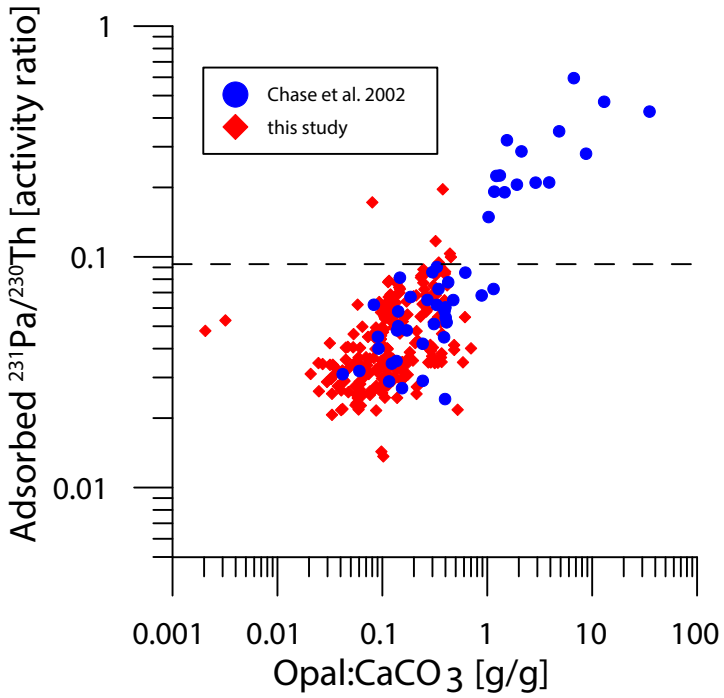
Chase et al. 2002
this study
Adsorbed $^{231}Pa/^{230}Th$ [activity ratio]
1
0.1
0.01
0.001
0.01
0.1
1
10
100
Opal:$CaCO_3$ [g/g]

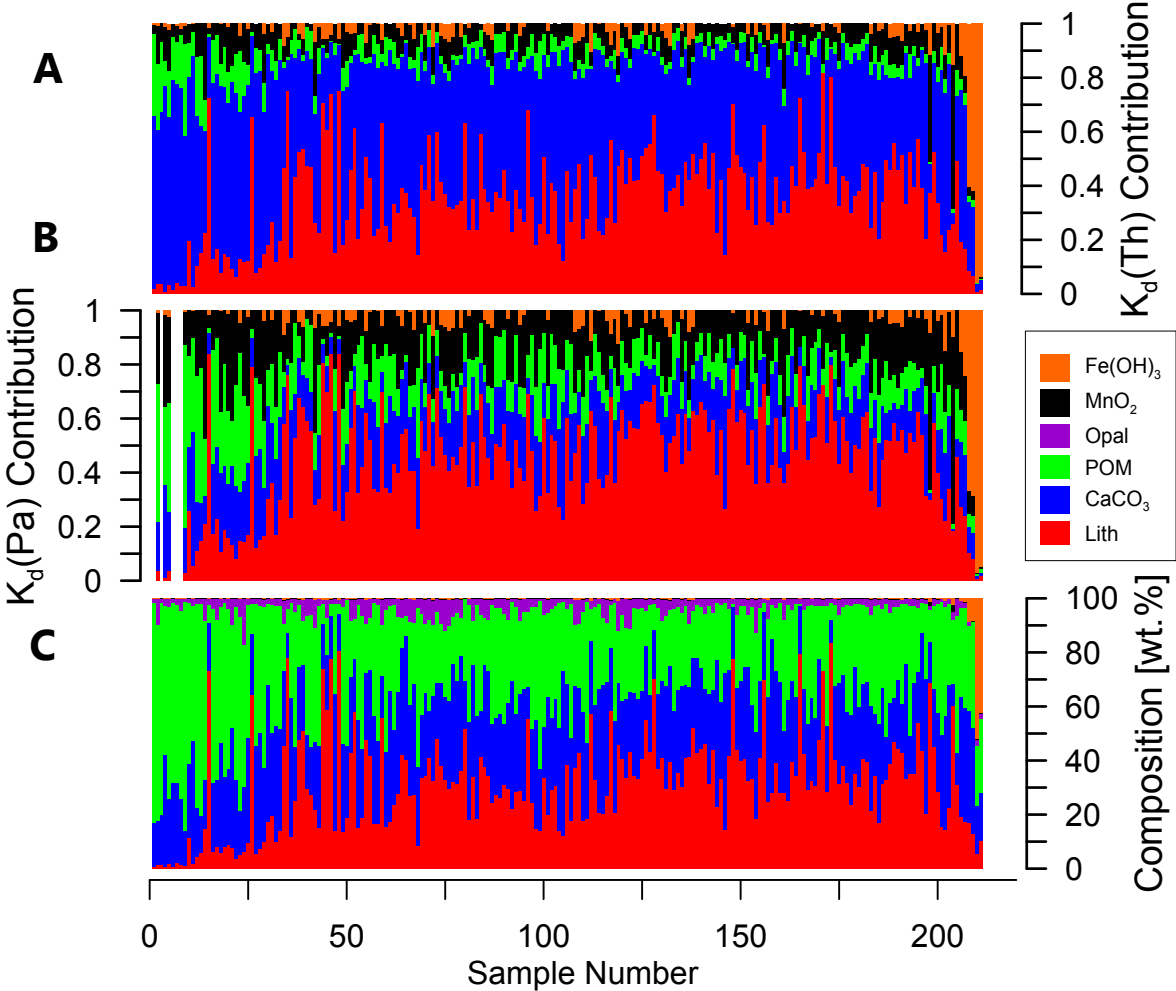
A
B
C
K_d(Th) Contribution
K_d(Pa) Contribution
Composition [wt.%]
Sample Number
$Fe(OH)_3$
MnO_2
Opal
POM
$CaCO_3$
Lith
0
0.2
0.4
0.6
0.8
1
0
20
40
60
80
100
0
50
100
150
200

Figure captions for Supplemental Material

Figure S1. Vertical sections along GA03, the U.S. GEOTRACES North Atlantic transect (as in Figs. 2, 5) of (A) adsorbed particulate ^{230}Th, (B) adsorbed particulate ^{231}Pa and the percentage composition of total particulate (C) ^{230}Th and (D) ^{231}Pa which is "detrital", or found within mineral lattices (as opposed to scavenged from seawater). Several points are labelled where values exceed the color bar ranges.

Figure S2. Cross-plots of K_d(Th) versus the particulate matter content of (A) lithogenic material, (B) opal, (C) $CaCO_3$, (D) particulate organic matter, (E) manganese oxides, and (F) iron hydroxides (F). Plot insets denote the Pearson linear correlation coefficient (r) and two-tailed p-value (statistical significance is usually attributed when p is less than 0.05). Note, however, that negative correlation coefficients are not physically meaningful as this would imply a negative K_d for pure phases. These apparent negative relationships must arise from the mixing of phases with different scavenging affinities. We therefore refer the reader to the non-negative, multiple least squares regression presented in the main text with regard to attributing scavenging intensity to specific phases.

Figure S3. Cross-plots of K_d(Pa) versus the particulate matter content of (A) lithogenic material, (B) opal, (C) $CaCO_3$, (D) particulate organic matter, (E) manganese oxides, and (F) iron hydroxides. Plot insets denote the Pearson linear correlation coefficient (r) and two-tailed p-value (statistical significance is usually attributed when p is less than 0.05). Note, however, that negative correlation coefficients are not physically meaningful as this would imply a negative K_d for pure phases. These apparent negative relationships must arise from the mixing of phases with different scavenging affinities. We therefore refer the reader to the non-negative, multiple least squares regression presented in the main text with regard to attributing scavenging intensity to specific phases.

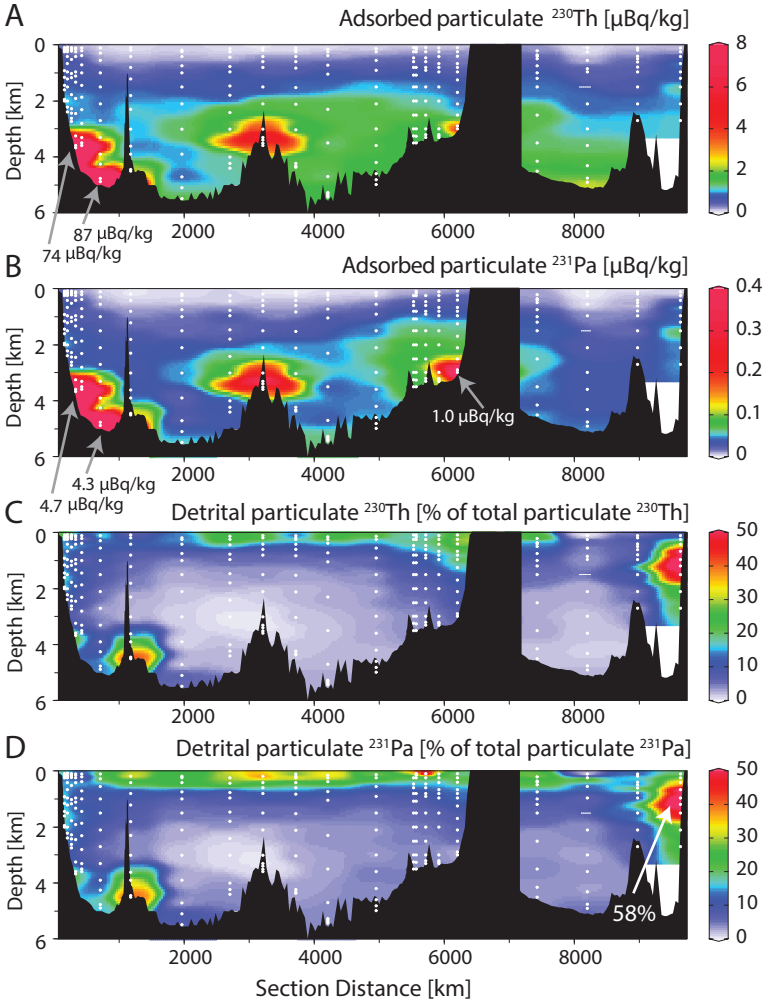
A
Adsorbed particulate ^{230}Th [µBq/kg]
Depth [km]
87 µBq/kg
74 µBq/kg
B
Adsorbed particulate ^{231}Pa [µBq/kg]
1.0 µBq/kg
4.3 µBq/kg
4.7 µBq/kg
C
Detrital particulate ^{230}Th [% of total particulate ^{230}Th]
D
Detrital particulate ^{231}Pa [% of total particulate ^{231}Pa]
58%
Section Distance [km]

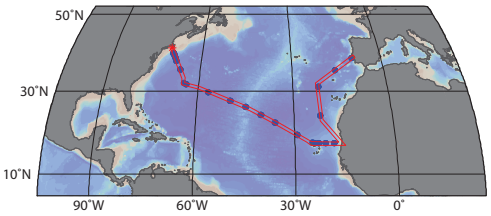
50°N
30°N
10°N
90°W
60°W
30°W
0°

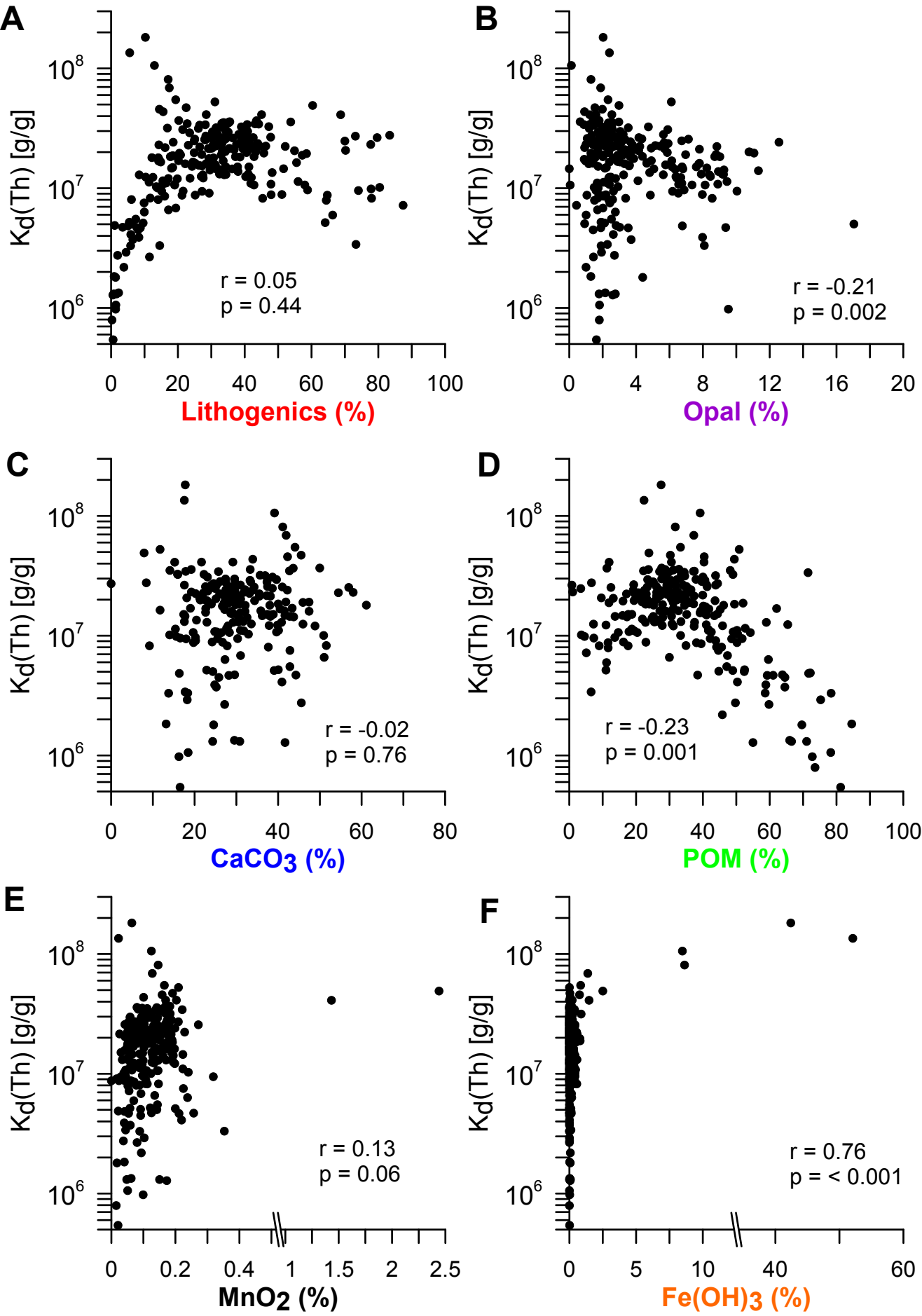
A
B
C
D
E
F
K_d(Th) [g/g]
10^8
10^7
10^6
r = 0.05
p = 0.44
0 20 40 60 80 100
Lithogenics (%)
r = -0.21
p = 0.002
0 4 8 12 16 20
Opal (%)
r = -0.02
p = 0.76
0 20 40 60 80
$CaCO_3$ (%)
r = -0.23
p = 0.001
0 20 40 60 80 100
POM (%)
r = 0.13
p = 0.06
0 0.2 0.4 1 1.5 2 2.5
MnO_2 (%)
r = 0.76
p = < 0.001
0 5 10 40 60
$Fe(OH)_3$ (%)

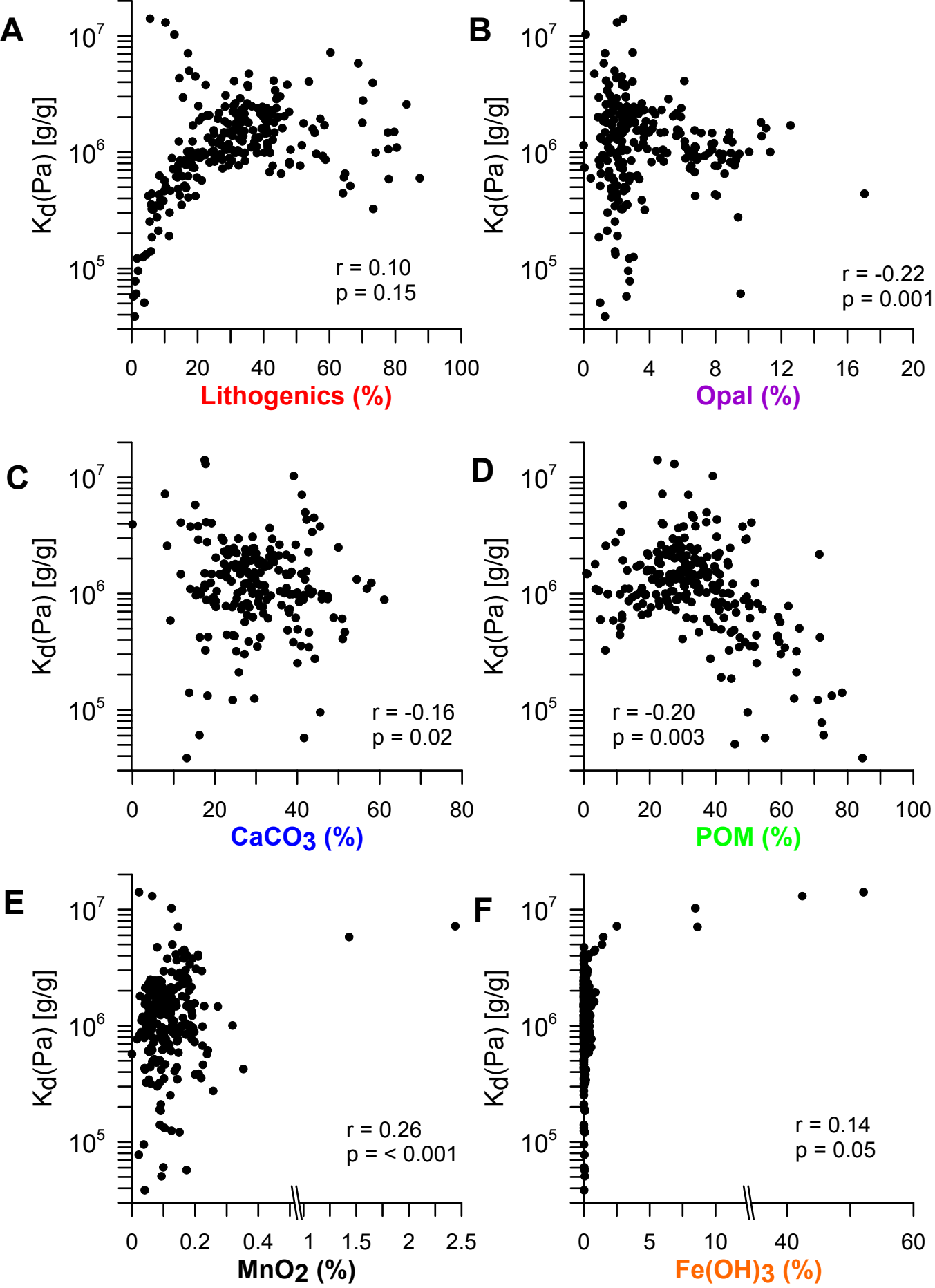
A
B
C
D
E
F
K_d(Pa) [g/g]
10^7
10^6
10^5
r = 0.10
p = 0.15
0 20 40 60 80 100
Lithogenics (%)
r = -0.22
p = 0.001
0 4 8 12 16 20
Opal (%)
r = -0.16
p = 0.02
0 20 40 60 80
$CaCO_3$ (%)
r = -0.20
p = 0.003
0 20 40 60 80 100
POM (%)
r = 0.26
p = < 0.001
0 0.2 0.4 1 1.5 2 2.5
MnO_2 (%)
r = 0.14
p = 0.05
0 5 10 40 60
$Fe(OH)_3$ (%)